Effects of electroweak phase transition dynamics on baryogenesis and primordial nucleosynthesis

Andrew F. Heckler
Fermilab National Accelerator Laboratory, Mail Stop 209, P.O. Box 500, Batavia, Illinois 60510
(Received 25 July 1994)

The evolution of the electroweak phase transition, including reheating due to the release of latent heat in shock waves, is calculated for various values of as yet unknown parameters of electroweak theory such as latent heat and bubble wall surface tension. We find that, for a wide range of parameter space, the bubble walls of the phase transition slow down by as much as a few orders of magnitude. Consequently, we also show that since baryon production can be a sensitive function of bubble wall velocity, it is important to include the effects of reheating in the calculation of the baryon density of the Universe. We show that there is a sensitive velocity dependence for all mechanisms of baryon production, depending on the magnitude of velocity of the bubble wall, and we examine in particular an inverse velocity dependence on baryon production, which is predicted by the charge transport mechanism of baryon production. For this mechanism we find both an enhancement of baryon production and the generation of inhomogeneities during the electroweak phase transition. We calculate the magnitude of the baryon enhancement, which can be as large as a few orders of magnitude, depending on the parameters of the theory, and we calculate the size and amplitude of the inhomogeneities generated. We determine that the inhomogeneities generated in a thermally nucleated electroweak phase transition are too small to survive diffusive processes and affect the nucleosynthesis epoch. We also examine the possibility that a phase transition nucleated by other means, such as by the presence of cosmic strings, may produce inhomogeneities that could affect nucleosynthesis.

PACS number(s): 98.80.Cq, 47.75.+f, 98.80.Ft

I. INTRODUCTION

The present calculations of baryogenesis in the electroweak (EW) phase transition do not include the effect of reheating due to the release of latent heat. In this paper, we will show that it is important to include this effect because reheating can dramatically affect the evolution of the phase transition. As a consequence, not only can the production of baryons be affected by a factor of as much as a few orders of magnitude, but also inhomogeneities in baryon density are generically produced.

To begin our discussion, let us first briefly describe the EW phase transition. First of all, in this paper we will *assume a first-order phase transition*, because this is the type that has the greatest chance of leaving observable remnants (i.e., baryons and inhomogeneities). Whether or not the EW phase transition is first or second order (or if there is any transition at all) is still an unresolved matter [1], though the present bias is toward a first-order transition. A first-order phase transition proceeds in the following way. When the Universe is at a temperature above the critical temperature T_c, the plasma is in its high-temperature unbroken (u) phase. As the Universe expands, it cools down below the critical temperature and bubbles of the low-temperature broken (b) phase begin to nucleate. Once a bubble has nucleated, it will begin to grow and its bubble wall velocity will quickly reach some velocity v_0, which depends on the temperature of the plasma and the internal bubble wall dynamics. As the bubbles grow and convert the plasma to the low-temperature phase, they will also release a certain amount of latent heat L, which is an (as yet) unknown parameter of EW theory, and this will tend to heat the plasma toward T_c. This reheating will in turn decrease the bubble wall velocity, which goes to zero as $T \to T_c$. If $L \ll \rho(T_c) - \rho(T_n)$, where T_n is the temperature at which the bubbles nucleate and ρ is the energy density, then the bubble walls will only slightly slow down. If $L \sim \rho(T_c) - \rho(T_n)$, then we will show that the bubble wall will slow down drastically ($v_0 \ll 1$) until the expansion of the Universe itself can absorb the latent heat (see, e.g., [2]). Of course, the picture is more complicated than this because the reheating is not homogeneous, but qualitatively this description is accurate.

The effect on the production of baryons originates from the observation that there is a sensitive bubble wall velocity dependence for all mechanisms of baryon production (the sensitivity depends on the magnitude of velocity of the bubble wall). Since the bubble walls decelerate as a result of reheating, we will find that baryon production can be enhanced by a large factor for a large range of parameters, such as latent heat and bubble wall surface tension, of the EW theory. This enhancement is independent of parameters such as the strength of CP violation, and so the observational constraints on these factors can be relaxed.

The bubble wall deceleration will also naturally produce inhomogeneities in baryon density that can have large amplitudes, depending on the parameters of EW theory. Since the production of elements at later times is

 ©1995 The American Physical Society

sensitive to inhomogeneities, we ask the important question, can certain regions of EW parameter space be ruled out, not only by careful measurements of the baryon density of the Universe, but also by constraints on inhomogeneities allowed by big bang nucleosynthesis calculations and observations? We will find that the inhomogeneities produced in a thermally nucleated EW phase transition are too small to survive important diffusive processes, and so the inhomogeneities do not play a significant role in big bang nucleosynthesis. However, we also examine the possibility of nonthermal nucleation (seeding) of the phase transition, which allows larger size inhomogeneities that can affect big bang nucleosynthesis.

It is important to note that in this paper we also investigate several important side issues in this large topic. For example, we must justify our assumption that baryon production is sensitively dependent on the velocity of the bubble walls. Also, since the velocity of the bubble walls is crucial not only for the calculation of baryon production, but also for the calculation of the phase transition dynamics, we will investigate in detail a method for calculating the velocity of the bubble walls which uses a damping coefficient η as a free parameter [3]. In this calculation of wall velocity, we have included several important effects previously neglected by many authors.

We should mention here that, so far, we have referred to *the* EW theory, when in fact there are many different EW theories (see [1] for a review). However, we will find that the calculations in this paper are not sensitive to the particular type of theory chosen. The only assumption we make is that the baryon production is sensitive to the velocity of the bubble wall, and we will see that this is true independent of the particular EW theory used. Since at times we will need to use specific examples in order to get numerical results, we will use what is called the "minimal" standard model EW theory, keeping in mind that our conclusions will still apply for other theories.

The structure of the paper is as follows. First of all, the reader who is only interested in the final results of the evolution of the phase transition, the resultant baryon production, and the effects on nucleosynthesis can refer directly to Secs. V–VII.

In Secs. II–IV we discuss the important detailed calculations that lead up to our results. For example, in Sec. II we investigate in detail how baryon production depends on the velocity of the bubble walls, and in Sec. IV we discuss the propagation of the bubble wall in detail. Finally, the last section summarizes the main conclusions of this paper.

II. ELECTROWEAK BARYOGENESIS

The quantum field theoretical aspects of EW baryogenesis are well developed, and so we refer the interested reader to a recent review of EW baryogenesis by Cohen, Kaplan, and Nelson [1]. The important point that we wish to use from the study of EW baryogenesis is that the third of Sakharov's conditions for baryogenesis, namely, that baryogenesis requires an out-of-equilibrium environment, is met via the EW phase transition [4].

In fact, it is the bubble walls that meet Sakharov's third and final requirement for baryogenesis: The plasma in and immediately around the bubble wall is out of equilibrium. Therefore the bubble wall plays an important role in baryon production. However, baryon production need not occur in the bubble wall itself. For example, transport processes can cause the region in front of the bubble to be out of equilibrium, thus allowing baryogenesis to occur in front of the bubble wall [5,6]. There are other mechanisms, such as spontaneous baryogenesis, which produce baryon number inside the bubble wall [7,8]. Exactly which mechanism dominates and where most of the baryons are created depend upon parameters such as the bubble wall thickness and bubble wall velocity [1,6].

The dominant baryon production mechanism will in turn more precisely determine how baryon production depends on the bubble wall velocity. We will see that the velocity dependence is important for determining the effects of phase transition dynamics on the total baryon density and on the production of inhomogeneities. So let us now examine the velocity dependence of baryon production more closely.

A. Bubble wall velocity and baryogenesis

The crucial assumption of this paper is that the baryon production rate is a sensitive function of bubble wall velocity for at least some range of velocities.

What is our justification for this assumption? How can we even justify that baryon production has *any* dependence on the bubble wall velocity? Strictly speaking, there is no question that baryon production in the EW phase transition depends on the bubble wall velocity v_0. How sensitive a function it is of velocity, however, depends on both the (dominant) mechanism of baryon production and the magnitude v_0. For example, in the limit that $v_0 \to 0$ (and keeping the bubble wall thickness constant) the plasma in and near the bubble wall remains in thermal equilibrium, and thus no baryon number is produced, independent of the mechanism of production. As the v_0 increases from zero, however, we will see that the velocity dependence of baryon production depends on which mechanism of baryon production is dominant.

In order to determine which mechanism of baryon production is dominant, one must compare three different time scales [1]: the thermal time scale $\tau_T \sim \text{few}/T$, the baryon violation time scale $\tau_B \sim 1/\alpha^4 T$, and the time scale of the wall, $\tau_w \sim \delta_w/v_0$, where δ_w is the bubble wall thickness. Nonetheless, we will find that all baryon production mechanisms have some common velocity-dependent characteristics at small and large velocities. Before we discuss these general characteristics, let us first take a close look at a specific mechanism in order to see how the bubble wall velocity dependence of baryon production is determined in detail.

1. Charge transport mechanism

In order to quantitatively calculate the effects of phase transition dynamics on baryon production, we will choose a model a baryon production based on the charge transport mechanism, which predicts that the baryon production is inversely proportional to the bubble wall velocity [5,6]. That is to say, our model for the calculation of baryon density $n_B(t)$ produced at some time t during the phase transition consists of one equation

$$n_B(t) = \frac{\mathcal{A}}{v_0(t)} , \tag{1}$$

where $\mathcal{A}$ is some constant which depends on the specific parameters of the theory of baryon production. For example, $\mathcal{A}$ is proportional to the amount of CP violation in the theory. Because we are grouping all of our ignorance about these parameters in $\mathcal{A}$, we will not be able to calculate absolute numbers for the total baryon density, but only numbers relative to some particular theory of baryon production represented by $\mathcal{A}$. In this way, we can isolate the effects of phase transition dynamics on baryon production, since previous authors neglected to take into account the changing velocity of the bubble walls during the phase transition.

We choose to use the charge transport mechanism as a model because it is a well-developed, plausible theory which has an explicit prediction of the bubble wall velocity dependence [5,6]. Let us examine in more detail the charge transport mechanism in order to determine how the velocity dependence of Eq. (1) comes about. Indeed, one might suspect that this velocity dependence must break down for small velocities, since for $v_0 \to 0$ this formula predicts infinite baryon density. We will find, as Nelson, Kaplan, and Cohen [5] have, that Eq. (1) is valid only for velocities above some cutoff velocity $v_{\rm co}$, which we will calculate. In this paper, we will also go one step further and determine the velocity dependence of baryon production as the bubble wall velocity $v_0 \to 0$.

The charge transport mechanism can be described in the following way. As the bubble wall propagates through the plasma, some kind of charge Y (e.g., lepton charge or hypercharge) is reflected off the bubble wall in a CP-violating way back into the high-T phase. This excess charge is then converted into baryon number via the previously mentioned baryon-number-violating processes continuously occurring in the high-temperature phase. At some point, the wall will again catch up to the charge, which is slowly diffusing through the plasma, and as the wall sweeps through the charge at this point, the baryon-number-violating processes will turn off (because they are exponentially suppressed in the low-T phase), leaving behind a baryon remnant.

Nelson, Kaplan, and Cohen [5] have shown that the rate per volume at which the charge Y is turned into baryon number, or what we call the baryon number density creation rate $\dot{n}_B|_{\rm cr}$ at some point z in space is

$$\dot{n}_B|_{\rm cr} = \frac{\mathcal{N}\Gamma_B}{T^3} n_Y(z - v_0 t) , \tag{2}$$

where $\mathcal{N}$ is a number of order unity which depends on the type of charge Y and on the number of Higgs scalars in the theory, Γ_B is the baryon violation rate per volume, and $n_Y(z - v_0 t)$ is the (steady state) charge Y number density for a wall moving with velocity v_0, for a point $z - v_0 t$ away from the wall.

However, since baryon number violation processes are continuously occurring, any baryon number that is created will also tend to equilibrate to its equilibrium value, which is zero. This behavior can be described by a "baryon number annihilation rate" $\dot{n}_B|_{\rm ann}$, which can be approximated by using a simple form of the Boltzmann equation

$$\dot{n}_B|_{\rm ann} \approx -\frac{n_B}{\tau_B} , \tag{3}$$

where, as stated before, τ_B is the baryon number violation time scale.

Putting these two rates together and making the rough approximation that $\tau_B^{-1} \approx \Gamma_B/T^3$, one obtains a formula for the total change in baryon number density:

$$\begin{aligned} \dot{n}_B &\approx \frac{\Gamma_B}{T^3}[\mathcal{N} n_Y(z - v_0 t) - n_B] \\ &\approx \frac{1}{\tau_B}[\mathcal{N} n_Y(z - v_0 t) - n_B] . \end{aligned} \tag{4}$$

The total baryon density at z can be found by integrating (4) over time. We will examine two limits of this formula in order to determine its behavior. The first limit is when $n_Y \gg n_B$, and the second limit is when $n_Y \ll n_B$. We will see that these two limits are equivalent to the large and small velocity limits of the bubble wall.

The first limit $n_Y \gg n_B$ occurs when the average time $\tau_{\rm ave}$ the charge Y spends out in front of the wall after being reflected (and before being caught again by the wall) is much smaller than τ_B. In this case, the charge Y has not had very much time to be converted into baryon number, and so n_B is small compared to n_Y. In this limit, one can neglect the n_B term in (4) and integrate over time. But first, in order to do this, one must calculate $n_Y(z - v_0 t)$. Since the charges thermalize in a few mean free paths, we can find an approximation to n_Y by using the diffusion equation. Since the wall is a constant source of reflected charge flux, we can approximate the flux as $J_Y \approx s_0 J_0(v_0)\delta(z - v_0 t)$, where s_0 is the characteristic distance a particle travels before it thermalizes and starts to random walk (e.g., see [6], or simply replace the δ function with $\exp[s_0(z - v_0 t)]^2/s_0$ to get a finite width source). Here we have explicitly noted that J_0 is a function of bubble wall velocity. The equation of diffusion of charge Y is then

$$\dot{n}_Y + D n_Y'' = s_0 J_0(v_0)\delta'(z - v_0 t) , \tag{5}$$

where D is the diffusion coefficient. One can obtain an approximate solution to Eq. (5) by observing that *outside* a distance s_0 from the wall the solution must be of the form $n(z) = n_0 e^{-v_0 z/D}$. In order to find n_0, one must use the boundary condition that at the wall the density is constant; therefore, using Eq. (5) we find $n(0) = s_0 J_0/D$, and so

$$n_Y(z) \approx \frac{s_0 J_0(v_0)}{D} e^{-v_0 z/D} . \quad (6)$$

The integrated baryon density in the case $n_Y \gg n_B$ or (as described above), equivalently, $\tau_B \gg \tau_{\rm ave}$, is then

$$n_B = \frac{\mathcal{N}\Gamma_B}{T^3} \int_{-\infty}^{z/v_0} dt\, n_Y(z - v_0 t) = \frac{\mathcal{N}\Gamma_B}{T^3} \frac{s_0 J_0(v_0)}{v_0^2} . \quad (7)$$

The velocity dependence of $J_0(v_0)$ is complicated (see [5] for an explicit expression), but to first order in v_0, $J_0 \propto v_0$. Therefore, in the limit $\tau_B \gg \tau_{\rm ave}$, we can see that $n_B \propto v_0^{-1}$, just as in Eq. (1).

In the second limit $n_Y \ll n_B$, however, the velocity dependence is very different. This limit occurs when $\tau_{\rm ave} \gg \tau_B$, giving the reflected charge Y plenty of time to convert to baryon number such that n_Y becomes small compared to n_B. In this case, one can solve for the total baryon density by assuming that all of the charge Y has converted into baryon number, and so we neglect the n_Y term when integrating Eq. (4). In this limit, the formula for the total baryon density is simply $\dot{n}_B = -n_B/\tau_B$. Of course, the exact solution of this equation will be complicated because the charges are not distributed evenly out from the wall, but the general behavior of the solution is of the form

$$n_B \approx n_{B0} e^{-\tau_{\rm ave}/\tau_B} , \quad (8)$$

where n_{B0} is an average the baryon number density, averaged over the inhomogeneous distribution of the initial Y charges that have been converted into baryon number. One would expect n_{B0} to be roughly the same as the baryon density calculated in the previous limit, namely, Eq. (7). Recall that $\tau_{\rm ave}$ is the average amount of time the charges stay in front of the wall after reflection. This average time can be estimated by observing from Eq. (6) that the distribution of Y charges diffuses out an average distance D/v_0 from the wall after reflection. Therefore it will take the wall an average time of

$$\tau_{\rm ave} \approx \frac{D}{v_0^2} \quad (9)$$

before the wall catches up again with the reflected charges.

We can approximate the velocity dependence of n_B in the $\tau_{\rm ave} \gg \tau_B$ limit by combining Eqs. (8) and (9) and by using the approximation of setting n_{B0} equal to the value of n_B in Eq. (7) to obtain

$$n_B \approx \frac{\mathcal{N}\Gamma_B}{T^3} \frac{s_0 J_0(v_0)}{v_0^2} e^{-D/(v_0^2 \tau_B)} \propto \frac{e^{-D/(v_0^2\tau_B)}}{v_0} , \quad (10)$$

where we have used $J_0 \propto v_0$. Notice that $n_B \to 0$ as $v_0 \to 0$, as it should.

Now that we have obtained the velocity dependence of n_b in two different limits, for what range of velocities are these two limits valid? First of all, Eq. (9) explicitly shows that is is completely equivalent to present the limits $\tau_{\rm ave} \ll \tau_B$ and $\tau_{\rm ave} \gg \tau_B$ as lower and upper bounds on the bubble wall velocity. For example, one can use (9) to express the limit $\tau_{\rm ave} \ll \tau_B$ as $v_0^2 \gg D/\tau_B$. Thus we can place a lower cutoff limit $v_{\rm co}$ on the bubble wall velocity for which the approximation $n_B \propto v_0^{-1}$ is valid. Recalling that $\tau_B \approx 1/(\alpha_W^4 T)$, we obtain

$$v_{\rm co}^2 \approx \alpha_W^4 T D . \quad (11)$$

For velocities less than this cutoff velocity $v_{\rm co}$, Eq. (10) is the valid form for n_B. The diffusion coefficient is typically equal to a few mean free path lengths λ. One should be careful to note that at these high temperatures there are many different types of particles to scatter off of (gluons, quarks, etc.), and so $\lambda \sim (N\alpha^2 T)^{-1}$, where N is the number of degrees of freedom in the plasma. This results in a mean free path $\lambda \approx$ few $\times T^{-1}$ [1]. We then estimate the cutoff velocity to be

$$v_{\rm co} \sim \alpha_W/\sqrt{N} \sim 10^{-3} , \quad (12)$$

but because of the theoretical uncertainties of quantities such as τ_B and D, the cutoff velocity could range anywhere from $10^{-4} < v_{\rm min} < 10^{-2}$. (Note here that Liu, McLerran, and Turok [25] have made a similar estimate of the minimum velocity, but they did not include the factor of $\sqrt{N}$.) The estimate (12) will be used as a reference value throughout the paper. For example, we will see that this limit is important for establishing the maximum allowable overdensities produced during the phase transition. Later in this paper, we will find out that *phase transition dynamics* will also place lower limits on bubble wall propagation velocities, and these limits will be of the same order as (12).

2. *General velocity dependence of baryon production*

Besides the specific example of the charge transport mechanism, one can make some remarks on the general characteristics of the velocity dependence of *any* mechanism of baryon production. For example, in the limit of very slow bubble wall velocities, the Boltzmann equation for the annihilation of baryon number, $\dot{n}_B = -n_B/\tau_B$, will play a major role in any baryon production mechanism. Just as we saw for the charge transport mechanism, this leads to a decrease in the baryon number of the form

$$n_B \approx n_{B0} e^{-\tau_{\rm ave}/\tau_B} , \quad (13)$$

where $\tau_{\rm ave}$ is the average time the baryon charges are exposed to the equilibrating (toward zero) baryon violation processes. For every mechanism, $\tau_{\rm ave}$ will be some monotonically decreasing function of v_0. If we assume that $\tau_{\rm ave} = D_0/v_0^n$, where D_0 is a characteristic length scale of the particular mechanism and the exponent n is also dependent on the particular mechanism, we find a general behavior in the small velocity limit:

$$n_B \propto e^{-D_0/(v_0^n \tau_B)} , \quad (14)$$

which goes to zero as $v_0 \to 0$. Note that, as in the charge transport mechanism, there could also be a velocity-dependent coefficient (of some power of v_0) multiplied onto this exponential dependence, but the exponential is the dominating behavior of n_B at small velocities.

In the large velocity limit $v_0 \to 1$, baryon production must also go to zero for every mechanism. This is because, for a given bubble wall thickness δ_w, the time $\tau_w = \delta_w/(\gamma v_0)$ that a given point in the plasma experiences out-of-equilibrium conditions will go to zero as $v_0 \to 1$ (due to Lorentz contraction of the wall), and when $\tau_w \ll \tau_B$, the velocity will be so fast that the baryon violation processes will not have time to create any baryons.

Putting these two limits together, we conclude that for *every* mechanism of baryon production, there is a velocity range for which n_B monotonically increases with v_0, and there also a velocity range for which n_B monotonically decreases with v_0. And for the case of small velocity, Eq. (14) indicates that n_B is an exponentially sensitive function of v_0. Figure 1 schematically presents the general velocity behavior for all mechanisms.

In summary, all models of bubble wall baryogenesis are dependent on the velocity of the bubble wall, and in at least some range of velocities they are *sensitively* dependent on the bubble wall velocity. We will find that, for some regions of parameter space, v_0 varies by a couple orders of magnitude during the phase transition. Therefore it is very plausible that v_0 will be in a range for which baryon production is sensitively velocity dependent, and phase transition dynamics will play an important role in baryon production. For this paper, we will concentrate on a model with a v_0^{-1} dependence because it is a generic feature of a wide class of models that work via the charge transport mechanism. However, we will make comments on a linear v_0 dependence also. One should keep in mind that since the phase transition dynamics are separate from baryon production, it is a simple matter to apply *any* velocity dependence of baryon production to the phase transition and calculate the average density and type of inhomogeneities produced.

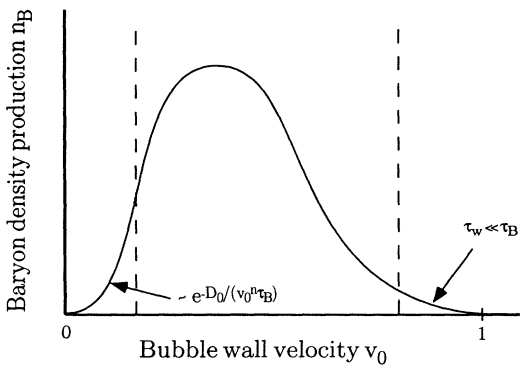

FIG. 1. Schematic picture (not to scale) of the general dependence of baryon production on bubble wall velocity. For small velocities, there is an exponential dependence. For velocities close the speed of light, baryon production is suppressed because time scales become too short for baryon-number-violating processes to create baryons. The velocity dependence in between the dashed line depends on the mechanism of baryon production. Here we have made a simple interpolation of what the velocity dependence might look like between the dashed lines. This shape is very similar to the velocity dependence of the charge transport mechanism examined in the text.

III. PHASE TRANSITION DYNAMICS

In this section, we briefly review some of the well-developed formulas necessary for calculating the dynamics of the phase transition. We also derive a formula for the total baryon density produced by the phase transition.

A. Higgs field potential

The scalar Higgs field ϕ is the order parameter of the phase transition. The EW phase transition corresponds to the passage of the vacuum expectation value of the Higgs field from zero to a nonzero value. The reader interested in a detailed discussion of the behavior of the Higgs field can refer to [9–12] and the references cited in [1]. In this paper, we will use a well-known approximation of the Higgs field potential in order to simplify our calculation [10–12]:

$$V(\phi,T) = A(T^2 - T_0^2)\phi^2 - BT\phi^3 + \frac{\lambda}{4}\phi^4 \,. \tag{15}$$

This approximation contains the essential features of the phase transition, namely, the general shape of two minima separated by a barrier. The actual shape of the potential may be slightly different than this (e.g., [13–15,11]), and one should keep in mind that small differences in the final numerical results may arise.

The high-temperature limit of the potential calculated from one-loop perturbation theory actually does take the form of (15), and the parameters A, B, T_0, and λ (which is weakly temperature dependent) can be put in terms of the zero-temperature masses of the Higgs boson, top quark, etc. Instead of this parametrization, we will choose to express A, B, T_0, and λ in terms of four parameters which are more physically descriptive of the phase transition: the latent heat L, the surface energy of the wall σ, the Higgs correlation length ξ (to leading order), and the critical temperature T_c [16,3]. This is a completely equivalent way of parametrizing (2), and these parameters are defined as

$$\begin{aligned}
L &\equiv T\frac{\partial V(\phi,T)}{\partial T}\bigg|_{\phi_0,T_c} = \frac{8T_0^4A^2B^2}{(\lambda A - B^2)\lambda} \,, \\
T_c &\equiv \frac{T_0}{(1 - B^2/\lambda A)^{1/2}} \,, \\
\xi &\equiv \left(\frac{\partial^2 V(\phi,T)}{\partial\phi^2}\bigg|_{\phi_0,T_c}\right)^{-1/2} = \frac{\sqrt{\lambda A - B^2}}{\sqrt{2A}T_0B} \,, \\
\sigma &\equiv \int \left(\frac{\partial\phi}{\partial x}\right)^2 dx\bigg|_{T_c} = \frac{2\sqrt{2}}{3}\frac{B^3T_0^3A^{3/2}}{\lambda(\lambda A - B^2)^{3/2}} \,,
\end{aligned} \tag{16}$$

where $\phi_0 = 2BT_0\sqrt{A}/[\sqrt{\lambda(\lambda A - B^2)}]$ is the value of the Higgs field (at T_c) at the second (low-T phase) minimum, and we calculated the function $\phi(x)$ using $V(\phi, T)$ in the equations of motion for $\phi(x)$. We will talk more about $\phi(x)$ in later sections.

In order to get an idea of the size of these parameters, one can refer to the perturbation theory (one-loop) calculation of the Higgs potential. In this theory, one can calculate the four parameters simply by knowing the mass of the Z and $W^{\pm}$ bosons, the mass of the top quark (the heaviest quark), and the mass of the Higgs boson [11]. The mass of the Z and $W^{\pm}$ are known, $M_Z \simeq 91$ GeV and $M_{W^{\pm}} \simeq 80$ GeV. The mass of the top quark is presently "known" (it has yet to be reliably detected) to about 20%, $M_t \approx 175$ GeV. The mass of the Higgs boson has an experimental lower bound of $M_H > 60$ GeV. Using these values (including $M_H = 60$ GeV), one obtains

$$L_0 \approx 0.14 T_{c0}^4 , \quad T_{c0} \approx 93.7 \text{ GeV} , \qquad (17)$$

$$\xi_0 \approx \frac{12.7}{T_{c0}} , \quad \sigma_0 \approx 0.0056 T_{c0}^3 ,$$

where the subscript zero stands for the one-loop calculation values. We will use these values as a reference point throughout the paper, though the whole point of this paper is to investigate all values of parameter space. Unless otherwise stated, these parameters in this paper will take these one-loop values.

B. Bubble nucleation

Now that we have the Higgs potential, we can calculate the mechanics of the phase transition. As the plasma cools down, the Higgs field, which is initially in the high-temperature unbroken phase, will become metastable, and it will eventually decay from the high-T phase to the low-T phase. The decay to the low-T phase is done via bubble nucleation.

A systematic theory of bubble nucleation from a metastable state has been developed by Langer [17]. Others have applied it to cosmological phase transitions [18,10]. Specifically, we will use the formula derived by Linde [10] for the nucleation rate per unit volume:

$$\Gamma_{\rm nuc}(T) = \kappa T \left(\frac{S_3(\phi, T)}{2\pi T}\right)^{3/2} e^{-S_3(\phi,T)/T} , \qquad (18)$$

where $S_3(\phi, T)$ is the three-dimensional action of the Higgs field. The constant κ is thought to be of order 1, and so we will set $\kappa = 1$.

Unfortunately, the calculation of the three-dimensional action $S_3(\phi, T)$ must be done numerically because there is no known analytical form. Dine *et al.* [11] have, however, found an approximation to $S_3(\phi, T)$ that takes a simple analytical form. This approximation assumes that $V(\phi, T)$ is of the form (15), and S_3 becomes a function of two parameters α and T:

$$\frac{S_3(\alpha, T)}{T} \approx \frac{4.85[2A(T^2 - T_0^2)]^{3/2}}{B^2 T^3} \times \left[1 + \frac{\alpha}{4}\left(1 + \frac{2.4}{1-\alpha} + \frac{0.26}{(1-\alpha)^2}\right)\right] , \qquad (19)$$

where

$$\alpha = \frac{\lambda[2A(T^2 - T_0^2)]^2}{2B^2T^2} . \qquad (20)$$

This function is accurate to a few percent in the whole interval of $0 < \alpha < 1$ (i.e., $T_0 < T < T_c$). We will use this approximation in all of the following calculations of the phase transition.

C. Fraction of space $F(t)$ occupied by the bubbles

Once the temperature of the Universe drops below the critical temperature T_c, bubbles of the new phase will begin to nucleate randomly in space, and as we will see in the next section, each bubble will immediately start to grow and fill up space. In order to calculate the volume of space occupied by the new phase, we will follow the prescription of Guth and Weinberg [19], where they find that at some time t the fraction of space $F(t)$ left in the high-temperature unbroken u phase is

$$F(t) = \exp\left\{-\frac{4\pi}{3}\int_{t_c}^{t} dt_1 \Gamma_{\rm nuc}(t_1)\left[\int_{t_1}^{t} dt_2 v(t_2)\right]^3\right\} , \qquad (21)$$

where $v(t_2)$ is the velocity of the bubble wall at time t_2. Note that we have neglected the initial radius of the bubble and the acceleration up to terminal velocity, because both of these effects are very small. We have also excluded the effects of the expansion of the Universe [10] because for all cases in this paper we will see that the duration of the phase transition is much less than the Hubble time. This formula for the fraction of space occupied does not take into account the dynamics of the colliding bubble walls, nor does it adequately describe the final moments of the transition (e.g., shrinking bubbles of an old phase). One should therefore keep in mind that Eq. (21) is only a convenient approximation (see [20] for a discussion).

D. Calculating the baryon density

One of the goals of this paper is to calculate the effect of the varying bubble wall velocity on the average baryon density of the Universe. Actually, we will not calculate the total baryon density, but rather the *ratio* of the total baryon density produced using a formula which accounts for variation in the bubble wall velocity, divided by the total baryon density produced assuming the bubble wall velocity is constant (which has been the standard assumption). The formula for this ratio is derived in the following way.

Let us define dB as the number of baryons produced in some volume element dV, where $V = [1 - F(t)]V_0$ is the volume of space that has been converted to the low-temperature b phase in some fiducial volume V_0.[1] Since $n_B = dB/dV$, we can use Eq. (1) to obtain

$$\dot{B} = -\frac{\mathcal{A}}{v(t)}\dot{F}V_0 \ , \tag{22}$$

where we have assumed that the expansion of the Universe is slow compared to the phase transition. We can then define a "baryon enhancement ratio" χ as the total number of baryons produced in V_0, accounting for the varying bubble wall velocity, divided by the number of baryons produced assuming constant wall velocity:

$$\chi \equiv \frac{B(v(t))}{B(v = v_0)} = -\int \frac{v_0}{v(t)}\dot{F}(t)dt \ , \tag{23}$$

where v_0 is the velocity of the bubble wall before it has been influenced by the presence of other bubbles. $B(v = v_0)$ is the number of baryons produced assuming the bubble wall velocity is constant at some v_0.

The explicit form of $\dot{F}(t)$ is

$$\dot{F}(t) = -4\pi v(t)\left(\int_{t_c}^{t} dt_1 \Gamma_{\rm nuc}(t_1)\left[\int_{t_1}^{t} dt_2 v(t_2)\right]^2\right) \times \exp\left\{-\frac{4\pi}{3}\int_{t_c}^{t} dt_1 \Gamma_{\rm nuc}(t_1)\left[\int_{t_1}^{t} dt_2 v(t_2)\right]^3\right\} . \tag{24}$$

Once we have a consistent calculation of the evolution of the phase transition, including the effect of reheating on $v(t)$, we can then apply Eq. (23) to find how the phase transition dynamics effect the final average baryon density of the Universe. The numerical results of Eq. (23) are presented in Sec. VI.

IV. BUBBLE WALL GROWTH

As seen from the last section, the determination of the bubble wall velocity is necessary for calculating both the phase transition dynamics and baryon production. Specifically, we must calculate the bubble wall velocity both before and during bubble wall collisions. These calculations are compounded by the following complication.

According to the laws of conservation of energy and momentum, there are two different ways a bubble wall can propagate: either as a deflagration or detonation. Simply put, for a growing bubble of low-temperature phase, nucleated in a plasma at rest, a deflagration is a propagating phase boundary preceded by a shock, and a detonation is a propagating phase boundary with no shock preceding it, but a rarefaction wave following it. For a complete discussion of these two cases, see Refs. [21–24]. [For a qualitative picture of the two cases, see Fig. 7 (Sec. V)].

Whether the bubble actually propagates as a detonation or a deflagration, however, is unambiguously determined by the internal dynamics of the bubble wall itself. Unfortunately, our knowledge of the EW phase transition is not detailed enough to reliably determine the internal dynamics of the bubble wall [25,11,26], and so we are still unsure whether it propagates as a detonation or deflagration. One can, however, *parametrize* the internal dynamics of the wall (e.g., see [3]). This is exactly what we will do in this section. We will employ a single parameter in the form of a damping coefficient η to describe the internal dynamics of the bubble wall.

This parametrization will allow us to determine which regions of EW (and damping coefficient) parameter space produce deflagrations and which produce detonations. It is important to distinguish between these two types of bubble wall propagation because, as we will see in the next section, they produce large quantitative and qualitative differences in the phase transition dynamics. We will concentrate on bubble walls propagating as deflagrations because we will find that a large region of parameter space (which easily includes the "expected EW values" of the parameters according to one-loop calculations) predicts that the walls will propagate as deflagrations. It is also the case that deflagrations produce the most interesting phase transition dynamics.

The parametrization of the internal dynamics of the bubble wall will also allow us to calculate the velocity of the bubble wall as a function of temperature, and this will be important when dealing with bubble collisions. First, though, let us begin with a general explanation of bubble wall growth.

A. Growth of the bubbles

Once a bubble has nucleated, it will start to grow because the pressure inside the bubble in the low-T phase is greater than in the high-T phase, and this difference is great enough to overcome the surface tension in the bubble walls. At first, the bubble walls will accelerate. If the bubble wall were "in a vacuum," then we could use the equation of motion of ϕ [see, for example, Eq. (27), ignoring the damping term] to estimate that the wall velocity would approach the speed of light in a time scale of $\tau \sim \phi_0^2/[\delta_w V(\phi_0, T)]$, where δ_w is the wall thickness. Typically, for the EW transition, this translates into $\tau \sim (10^2\text{–}10^4)(1/T)$, which shows that the bubble walls reach terminal velocity within a few hundred bubble wall widths, easily by the time it is macroscopic [and recall that the Hubble length H^{-1} at 100 GeV is $H^{-1} \sim M_{\rm Pl}/T^2 \sim 10^{17}(1/T)$, where $M_{\rm Pl}$ is the Planck mass]. The additional coupling of the Higgs field to the thermal plasma does not change the above conclusion that once a bubble is nucleated its wall will

[1] Since the time and distance scales for baryon production are much smaller than the macroscopic time and distance scales that the baryon density varies, the use of differentials is a good approximation.

quickly reach some terminal velocity v_0 (in fact, if ϕ is strongly damped, the wall will reach terminal velocity even faster). We will therefore ignore this initial acceleration stage of the bubble.

The important question is, what is the (terminal) velocity of the bubble wall? Presently, the answer is not known. The difficulty lies in the fact that the velocity of the wall is determined by internal dynamics of the bubble wall, namely, the interaction of the wall with the plasma.

To get a physical idea of bubble wall propagation, consider the following picture. As the wall sweeps through a specific point in the plasma, ϕ acquires a vacuum expectation value, and the particles that are coupled to ϕ (quarks, etc.) will acquire a mass. If ϕ changes fast enough, the particles which initially had a thermal distribution appropriate for their massless state will be out of thermal equilibrium because they now have a mass. The particles that have an initial energy lower than the new mass they should acquire cannot pass into the low-T phase, but rather are reflected, because they do not have enough energy to pass through the wall. The reflected particles will thus impart momentum to the wall and slow it down, and the faster the wall goes, the more momentum the particles will impart on the wall. With this picture, we can see that when the bubble wall propagates through a plasma, a frictional type of force opposes the motion.

However, if ϕ changes sufficiently slowly in time, then the particles will always be in thermal equilibrium in the wall and there will be no reflection and no velocity-dependent force [27]. The two parameters that determine how fast ϕ changes with time are the velocity of the wall v_0 and the bubble wall thickness δ_w. If the time scale for the change in ϕ is much greater than the thermal time scale, $\delta_w/v_0 \gg \tau_{\rm th}$, then the velocity-dependent damping will turn off.

The above is the standard picture for analyzing the wall velocity [11]. More precisely, to estimate the terminal velocity, one uses the above picture to derive a formula which equates the pressure difference across the wall, which drives the expansion, with the leading-order velocity dependence of the frictional damping pressure

$$p_b - p_u = \mathcal{E} v_0 \ , \tag{25}$$

where b and u stand for the low- (broken) and high- (unbroken) T phases, respectively, and $\mathcal{E}$ represents the calculation of strength of reflection of the particles off the wall [11]. As explained above for $\delta_w/v_0 \gg \tau_{\rm th}$, the particles become more and more weakly reflected, and the right-hand side goes to zero [27]. In this paper, we will make two important changes to Eq. (25). The first change comes from the observation, as we will see in Sec. IV B, that $\delta p = p_b - p_u$ is *velocity dependent.* This is tied in with the second change: According to energy-momentum conservation, there *must* be a temperature difference across the wall (see Sec. IV B), contrary to what previous authors have assumed [27,11,25] (although, for example, Ignatius *et al.* [3] have correctly included this effect). These two changes will make a big difference in the calculation of the wall velocity. In a sense, this is another kind of damping on the bubble wall—a damping due to a temperature-dependent pressure difference across the wall. We will discuss this again at the end of this section.

Dine *et al.* [11] have made an estimate of the bubble wall velocity in EW theory using the above picture. Liu, McLerran, and Turok [25] have estimated the friction coefficient (for thin walls) by using a more analytical approach. They add corrections to the Higgs field from the loop expansion to the equation of motion of the Higgs field to obtain

$$\frac{d^2\phi}{dt^2} - \nabla^2\phi + \frac{dV}{d\phi} + \int d^4x' \ \Sigma(x,x')\phi(x') = 0 \ , \tag{26}$$

where Σ is the self-energy of the Higgs field. This extra term is responsible for the frictional force on the wall [comparing this equation with Eq. (27) in the next section makes this more clear]. All the authors that have estimated the wall velocity (e.g., [10,11,27,25]) reach the same general conclusion that thick walls have a larger velocity than the thin walls. The estimated velocities for thin walls are typically $v_{\rm thin} \sim 0.1$, but the estimates for thick walls are in the range $v_{\rm thick} \sim 0.1$–1.

B. Parametrization of the wall velocity

In this paper, we do not claim any value for the wall velocity v_0; rather, we parametrize v_0 with a damping coefficient η and explore the possible values of v_0 for a given η. This in effect sweeps all of the messy calculations of the internal dynamics of the bubble wall into one number η. The parametrization of v_0 is done by the following method.

The equation $\partial_\mu\partial^\mu\phi + \partial V/\partial\phi = 0$ is the classical equation of motion for ϕ with no damping. We will assume that the motion of the ϕ is damped and that this damping is proportional to $d\phi/dt$, which is the standard frictional damping assumption [28]. This damping will add a term to the equation of motion, $\eta d\phi/dt$. The Lorentz-invariant version of this term is $\eta u^\mu \partial_\mu\phi$ where u^μ is the four-velocity of the plasma. The equation of motion then becomes

$$\partial_\mu\partial^\mu\phi + \frac{\partial V}{\partial\phi} + \eta u^\mu \partial_\mu\phi = 0 \ . \tag{27}$$

This equation is also derived by Ignatius *et al.* [3] by using the stress-energy tensor of ϕ and the plasma and assuming some coupling between the two. (Note that we use η as a damping coefficient instead of $1/\Gamma$ used in their paper. We have chosen this convention because it is the standard damping factor convention.)

Before we go on with the calculation of the bubble wall velocity, let us mention here that η can be estimated by observing from (27) that the amount of energy per volume per second, $\dot{\epsilon}$, generated by the frictional damping is [28] $\dot{\epsilon} \approx \eta\dot{\phi}^2$. Multiplying this by the bubble wall thickness δ_w, one obtains an estimate of the amount of energy generated per area per second by the frictional damping. This must be equal to $\delta p v_0$, where δp is the pressure

on the wall due to the frictional damping and v_0 is the velocity of the bubble wall. Therefore

$$\eta \approx \frac{\delta p \delta_w}{\phi_0^2 v_0} , \tag{28}$$

where we have assumed that $\dot{\phi} \approx \phi_0 v_0/\delta_w$ and ϕ_0 is the value of the Higgs field in the broken phase. By using approximations for δp obtained from Refs. [27,11,16] as a guide, we roughly estimate that $\eta \sim g_W^2 T_c \approx 0.3 T_c$. This will be used as a reference value throughout the paper, and unless otherwise stated, η will assume this value.

Getting back to calculating the bubble wall velocity, because the bubble wall is so thin ($\ll$ radius of bubble), we can go to $1+1$ dimensions. If we boost to a frame moving with the wall (velocity v) and we assume that all processes have stabilized so that all time derivatives vanish, Eq. (27) becomes

$$\phi''(x) = \frac{\partial V(\phi,T)}{\partial \phi} + \eta v \gamma \phi'(x) , \tag{29}$$

where $\gamma = 1/(1-v^2)^{1/2}$. Furthermore, if we multiply both sides by $d\phi(x)/dx$ and integrate over $-\infty < x < +\infty$ [recall $\phi(\pm\infty) = \text{const}$], we obtain a formula for the velocity of the wall:

$$v\gamma = \frac{1}{\eta} \frac{\int_{\phi_b}^{\phi_u} \frac{\partial V(\phi,T)}{\partial \phi} d\phi}{\int \left(\frac{\partial \phi(x)}{\partial x}\right)^2 dx} . \tag{30}$$

Note that we have assumed that $v(x)$ is constant across the wall. In reality, $v(x)$ is not constant because the bulk fluid velocity is different on either side of the wall, but the change in velocity is of order $\delta T/T$ [see Eq. (39)], which is small, and so we will neglect it.

The integral in the numerator of (30) can be performed provided that $T(x)$ can be expressed in terms of $\phi(x)$. This is a natural assumption to make, because, since changes in quantities such as temperature and velocity of the plasma are driven by the phase transition, one would expect that these quantities would be functions of $\phi(x)$, which is the function that describes the evolution of the phase transition. Therefore we will assume that

$$T(x) = \frac{T_u + T_b}{2} + \frac{T_u - T_b}{2}\left(1 - 2\frac{\phi(x)}{\phi_b}\right) , \tag{31}$$

where b and u stand for the low- (broken) and high- (unbroken) temperature phase and ϕ_b is the value of ϕ at the minimum of $V(\phi,T)$, in the b phase. Note that ϕ_b is temperature dependent. A numerical, hydrodynamical simulation of bubble wall propagation, performed by Ignatius *et al.* [3], has shown that Eq. (3) is a good approximation; however, they have found that for some regions of EW parameter space the temperature profile is slightly shifted with respect to the $\phi(x)$, and $T(x)$ is also slightly different in shape than (3). A shift on the order of the Higgs correlation length ξ can drastically change the value of the numerator of the right-hand side of (30). We will talk more about this shift in Sec. IV D.

The denominator of the right-hand side of (30) is the surface tension of the bubble wall at T, $\sigma(T) = \int (\partial\phi/\partial x)^2 dx$. In order to calculate $\sigma(T)$, we must first find $\phi(x)$. We will simplify matters by assuming a specific form

$$\phi(x) = \frac{\phi_b}{2}\left[1 + \tanh\left(\frac{x}{n_w \xi}\right)\right] , \tag{32}$$

where n_w is the characteristic bubble wall thickness in units of correlation length ξ. In the limit that $T_b = T_u = T_c$ and $\eta = 0$, (32) is the exact solution to Eq. (29) [for $\phi(\infty) = 0$, $\phi(-\infty) = \phi_b$] with $n_w = 2$. In reality, n_w is a function of η and v, and we will keep it explicitly in the formulas, though for now, we will assume that $n_w \simeq 2$.

Combining Eqs. (30), (3), and (32), we obtain

$$\frac{v(T_b,T_u)}{[1-v(T_b,T_u)^2]^{1/2}} = \frac{n_w \xi}{8\lambda\eta}\left\{3BT_u\sqrt{9B^2T_b^2 - 8\lambda A(T_b^2 - T_0^2)} + [9B^2T_bT_u - 8\lambda A(T_bT_u - T_0^2)] + 4\lambda A(T_u^2 - T_0^2)\right\} \tag{33}$$

and, in the limit $T_u = T_b$,

$$\frac{v(T_b = T_u)}{[1-v(T_b = T_u)^2]^{1/2}} = \frac{n_w \xi}{8\lambda\eta}\left[3B^2T_b^2\left(1 - \frac{\sqrt{B^2T_b^2 + 8(\lambda A - B^2)(T_c^2 - T_b^2)}}{BT_b}\right) + 12(\lambda A - B^2)(T_c^2 - T_b^2)\right] , \tag{34}$$

which explicitly goes to zero as $T_b \to T_c$. There are two important points about Eq. (33). The first is that this formula is correct only to first order in $T_u - T_b$. That is, we solved for ϕ_b assuming that the temperature was uniform (T_b). The fact that the temperature varies from the unbroken phase to the broken phase will change the velocity by an amount of order $(T_u - T_b)/T_c$, which is small, and so we neglect it.

The second important point about Eq. (33) is that if $T_u > T_c > T_b$ or $T_b > T_c > T_u$, the wall will still propagate forward (see also [29,3]). The physical reason for this is that since the temperature is not uniform, the shape of the Higgs potential $V(\phi,T)$ is slightly different than in the uniform-temperature case. The shape of the potential changes in such a way that the broken phase can still have a lower free energy than the unbroken

phase *even if* $T_b > T_c > T_u$ (this is easier to imagine for $T_u > T_c > T_b$). Therefore the wall will propagate forward because it is energetically favored. This can be explicitly shown by inserting the formulas for $T(x)$ and $\phi(x)$ into $V(\phi, T)$. Of course, for the uniform-temperature case [Eq. (34)], the bubble wall stops at $T = T_c$.

Equation (33) brings us one step closer to determining the wall velocity, but this equation only gives the velocity in terms of T_b and T_u at the bubble wall. Given some bubble that nucleates in a plasma with an initial temperature T_n, how does one determine T_b and T_u at the bubble wall? First, let us assume there is no influence from neighboring bubbles (we will add this in later). As stated before, we can then impose conservation of energy and momentum on the bubble wall to constrain the propagation to two possible forms, namely, detonations or deflagrations. For a given damping coefficient η, Eq. (33) will allow only one or the other, and this will then determine the temperature on both sides of the wall. In the next section, we will concentrate on deflagration solutions.

Before we start the next section, let us just note here that, ideally, Eq. (29) should be solved numerically along with the equations from $\partial_\mu T^{\mu\nu} = 0$ (as in [3], though they do this in $1+1$ dimensions), to get $v(x)$, $T(x)$, and $\phi(x)$. Instead, we have used analytical approximations to get an expression for v, because this will make computing the rest of the phase transition easier.

C. More complete treatment of deflagration wall propagation

Previous authors have not applied spherical bubble propagation theory to the EW phase transition. There have been studies of planar wall propagation [29,2,30,3], but we will see that the spherical geometry of the bubbles plays a dominant role in determining the characteristics of the bubble wall propagation. Most notably, the shock fronts become extremely weak for spherical bubbles. We will use this fact to develop a useful and intuitive approximation that simplifies the calculation of the bubble wall velocity. This approximation is found to be very accurate in the case of the EW phase transition.

Let us note that we have also calculated the deflagration velocity for planar walls, and in a wide range of parameter space, the planar wall calculation is a good approximation to the spherical bubble deflagration, and the error is only $\lesssim$ 1–20 %. But for larger values of the latent heat L, the error can be as much as a factor of 2. We use the spherical bubble calculation because an accurate calculation of the bubble wall velocity is important for determining whether the walls travel as detonations or deflagrations and also for determining how the phase transition evolves.

The general picture of spherical deflagration wall propagation in a plasma is the following [23]. The deflagration front is preceded by a shock front, which travels at a velocity $v_{\rm sh} > c_s$, where $c_s = \sqrt{1/3}$ is the velocity of sound in a relativistic plasma. In front of the shock, we impose the boundary condition that the plasma is not moving and has temperature T_n, the temperature at which the bubble nucleated. Between the shock and deflagration front, the plasma has a temperature $T_u(z)$, which is greater than T_n, and bulk fluid velocity $v_{\rm fl}(z)$, where z is the distance from the bubble wall. It is important to stress that for spherical bubbles the temperature and fluid velocity of the plasma in front of the wall are both a function of distance from the bubble wall. Behind the deflagration front, we impose the boundary condition $v_{\rm fl} = 0$ and $T = T_b$.

The velocity of the deflagration front is determined by the conservation of energy and momentum, the equation of motion of ϕ, and the above boundary conditions [29,23]. The conservation of energy and momentum is best applied by using the well-known property of the stress-energy tensor $\partial_\mu T^{\mu\nu} = 0$. At a wall discontinuity, assuming a stationary solution and a perfect gas, one obtains [29]

$$\begin{aligned}(\rho_1 + p_1)\gamma_1^2 v_1 &= (\rho_2 + p_2)\gamma_2^2 v_2 \ , \\ (\rho_1 + p_1)\gamma_1^2 v_1^2 + p_1 &= (\rho_2 + p_2)\gamma_2^2 v_2^2 + p_2 \ ,\end{aligned} \tag{35}$$

where the subscripts 1 and 2 refer to either side of the wall. Solving for the deflagration front with the above boundary conditions, one obtains [29]

$$v_{\rm def} = \sqrt{\frac{(p_b - p_u^{\rm def})(\rho_u^{\rm def} + p_b)}{(\rho_b - \rho_u^{\rm def})(\rho_b + p_u^{\rm def})}} \ , \tag{36}$$

where p and ρ are defined by Eq. (47) and $p_u^{\rm def}, \rho_u^{\rm def}$ are the pressure and energy density in the u phase at the deflagration front [recall that $T_u(z)$ is a function of distance z from the bubble wall].

One can now use Eq. (33) and set $v(T_b, T_u^{\rm def}) = v_{\rm def}$, where $T_u^{\rm def}$ is the temperature of the plasma in the u phase at the deflagration front (recall that T_b is constant), in order to eliminate one unknown (T_b). The deflagration velocity is now a function of $T_u^{\rm def}$ only (for a given η, λ, etc.). What is the temperature $T_u^{\rm def}$ of the u phase at the deflagration front? It is not a free parameter; rather, it is determined by the boundary conditions at the shock front.

That is to say, one can solve (35) for the shock discontinuity (with the above boundary conditions) in order to obtain the fluid velocity of the plasma just behind the shock,

$$v_{\rm fl}^{\rm sh} = \sqrt{\frac{\rho_u^{\rm sh} - \rho_n)(p_u^{\rm sh} - p_n)}{(\rho_u^{\rm sh} + p_n)(\rho_n + p_u^{\rm sh})}} \ , \tag{37}$$

where the unshocked plasma n has the same equation of state as the unbroken u phase and $\rho_u^{\rm sh} \equiv \rho_u(T_u^{\rm sh})$, where $T_u^{\rm sh}$ is defined as the temperature of the plasma at the shock front.

However, one can also find the fluid velocity at the shock by starting with the fluid velocity at the deflagration front and then using the fluid motion equations ($\partial_\mu T^{\mu\nu} = 0$; see below) to find $v_{\rm fl}$ at the shock. These two different methods for calculating $v_{\rm fl}$ at the shock must agree. Since $v_{\rm fl}$ at the deflagration front is a function of

$T_u^{\rm def}$, one can make the two answers agree by adjusting $T_u^{\rm def}$. This fixes the value of $T_u^{\rm def}$ and therefore $v_{\rm def}$.

The formulas for the temperature and fluid velocity between the deflagration front and the shock are obtained by solving $\partial_\mu T^{\mu\nu} = 0$ for the case of spherical symmetry [23]. These equations are enormously simplified by assuming similarity solutions: $\rho = \rho(\xi)$, $p = p(\xi)$, $v_{\rm fl} = v_{\rm fl}(\xi)$, where, for radius r of the bubble and time t, $r/t = \xi$. This is a reasonable assumption, since we have assumed the walls have reached a steady state. With this simplification, the solutions become [23]

$$\frac{1}{\rho}\frac{d\rho}{d\xi} = 4\frac{\xi - v_{\rm fl}}{1-\xi v_{\rm fl}}\frac{1}{1-v_{\rm fl}^2}\frac{dv_{\rm fl}}{d\xi} ,$$

$$[v_{\rm fl}^2(3-\xi^2) - 4v_{\rm fl}\xi + 3\xi^2 - 1]\frac{dv_{\rm fl}}{d\xi} = 2\frac{v_{\rm fl}}{\xi}(1-v_{\rm fl}^2)(1-\xi v_{\rm fl}) . \quad (38)$$

By setting the boundary conditions $T(\xi = v_{\rm def}) = T_u^{\rm def}$ and $v_{\rm fl}(\xi = v_{\rm def}) = v_{\rm fl}^{\rm def}$, one can solve (35) to find

$$v_{\rm fl}^{\rm def} = \sqrt{\frac{(\rho_u^{\rm def} - \rho_b)(p_u^{\rm def} - p_b)}{(\rho_u^{\rm def} + p_b)(\rho_b + p_u^{\rm def})}} . \quad (39)$$

For $v_{\rm fl}^{\rm def} \ll 1$, one can use (38) to estimate the magnitude of the fluid velocity at the shock [23]:

$$v_{\rm fl}^{\rm sh} \lesssim \exp\left\{-\frac{\left(\frac{1}{v_{\rm def}^2} - 3\right)}{4\sqrt{3}v_{\rm fl}^{\rm def}}\right\} . \quad (40)$$

To get an idea of the magnitude of $v_{\rm fl}^{\rm sh}$, consider the values $v_{\rm fl}^{\rm def} = 3\times 10^{-3}$ and $v_{\rm def} = 0.5$. (Typically, since $T_u^{\rm def} - T_b \ll T_b$ for the EW phase transition, $v_{\rm fl}^{\rm def} \lesssim$ a few $\times 10^{-3}$.) Then we find that $v_{\rm fl}^{\rm sh} \lesssim 10^{-21}$. We can see that the shock front is *extremely* weak. This is due both to the fact that the phase transition itself is weak (i.e., the latent heat is small) and that the spherical geometry also drastically "damps" the strength of the shock wave.

The extreme weakness of the shock front is a generic characteristic of deflagration bubbles in the EW phase transition. There is an advantage to this characteristic: It will allow us to solve for $T_u^{\rm def}$, and ultimately $v_{\rm def}$, by using the following approximation.

First, consider the velocity of the shock front, $v_{\rm sh}$, for a weak shock. By solving (35) for the shock discontinuity, one obtains

$$v_{\rm sh} = \sqrt{\frac{(p_u^{\rm sh} - p_n)(\rho_u^{\rm sh} + p_n)}{(\rho_u^{\rm sh} - \rho_n)(\rho_n + p_u^{\rm sh})}} . \quad (41)$$

Since we have shown that $v_{\rm fl}^{\rm sh} \ll 1$, we can use (37) to estimate $v_{\rm fl}^{\rm sh} \approx \sqrt{3}(T_u^{\rm sh} - T_n)/T_n \ll 1$. We can then use (41) to estimate $v_{\rm sh} \approx [1 + (T_u^{\rm sh} - T_n)/T_n]/\sqrt{3}$. Therefore, since $v_{\rm fl}^{\rm sh}$ is so small,

$$v_{\rm sh} \approx \sqrt{1/3} \quad (42)$$

to a very good approximation (e.g., 1 part in $\sim 10^{20}$).

Now one can employ the conservation of energy to find $T_u^{\rm def}$. Consider the volume V_0 occupied by the entire bubble, including the shock front. Ignoring the expansion of the Universe, which is a small effect, the total energy inside that volume must be equal to its initial energy $E_{\rm tot} = \rho_n V_0$. But $E_{\rm tot}$ must be equal to the sum of the b phase part of V_0 and the u phase part that is shocked. Therefore

$$\tfrac{4}{3}\pi v_{\rm sh}^3 \rho_n(T_n) = \tfrac{4}{3}\pi v_{\rm def}^3 \rho_b(T_b) + 4\pi \int_{v_{\rm def}}^{v_{\rm sh}} \rho(\xi)\xi^2 d\xi . \quad (43)$$

Here we have neglected the kinetic energy of the fluid in the shock because $v_{\rm fl} \ll 1$. Since for a weak shock $v_{\rm sh} \approx \sqrt{1/3}$, the problem is now reduced to finding $\rho_u(\xi)$. In the limit $v_{\rm fl}^{\rm sh} \ll 1$, there is an analytical solution to (38) [23]:

$$\rho(\xi) \approx \rho_u(T_u^{\rm def}) e^{C(1/\xi - 1/v_{\rm def})} , \quad (44)$$

where $C = v_{\rm fl}^{\rm def}/(1/v_{\rm def}^2 - 3)$.

By setting $v_{\rm def} = v(T_b, T_u^{\rm def})$ and combining Eqs. (36), (43), and (44), one can numerically solve for $T_u^{\rm def}$ and $v_{\rm def}$. This method vastly simplifies the problem, because we are just left with essentially two equations [$v_{\rm def} = v(T_b, T_u^{\rm def})$ and (43)] and two unknowns $(T_b, T_u^{\rm def})$. The reason the problem is simplified is that the shock is weak and we can set $v_{\rm sh} = \sqrt{1/3}$, which eliminates the "third" unknown.

We have compared the results of this approximation with full numerical calculations [i.e., solving (36), (38), etc., directly], and we have found that the error in temperature $|(T_{\rm app} - T_{\rm full})/(T_{\rm full} - T_c)| < 1\%$ for $v_{\rm def} > 0.5$ (although, as $v_{\rm def} \to c_s$, this approximation breaks down), and the error is much smaller for smaller $v_{\rm def}$. These errors in temperature correspond to errors $< 1\%$ in the calculation of the deflagration velocity.

D. Numerical results of deflagration wall velocity

By numerically solving Eqs. (33), (36), and (43), we can calculate the velocity v_0 of the deflagration front as a function of the parameters of EW theory (L, ξ, σ, T_c) and the damping coefficient η. These numerical calculations enable us to verify whether our assumption that the bubble walls travel as deflagrations for a certain region of parameter space is self-consistent, i.e., that $v_0 < c_s$, since for detonations $v_0 > c_s$ [22]. We will also be able to determine the magnitude of the wall velocity so that we can get an idea which approximation (see the following sections) of the phase transition is the relevant one.

In Fig. 2 we have produced some typical bubble temperature profiles for a couple of values of L and η. Note that the smaller the damping η is, the higher both T_b and T_u are at the bubble wall. These higher temperatures will in turn prevent the velocity from becoming very large, because the closer T_b is to T_c and the closer T_u is to its maximum, the slower the velocity. In this way, we can see that there is not a simple dependence of v_0 on η. Likewise, larger latent heat will also slow

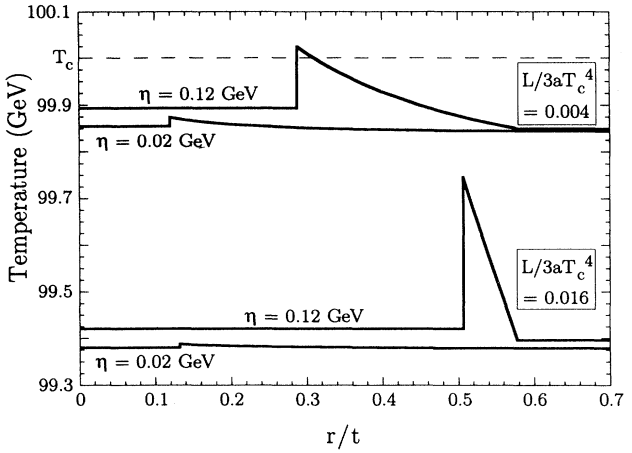

FIG. 2. Temperature profiles for spherical deflagration bubbles for various values of damping coefficient η and latent heat parameter $L' \equiv L/(3aT_c^4)$. The discontinuity in the temperature is the deflagration front: It is where the phase is changing from the unbroken phase to the broken phase. In front of the discontinuity is the shock front, where most of the latent heat is transported. Note that as the wall goes faster, more heat "bunches up" around the deflagration front. This shark-fin effect is responsible for a damping of the deflagration front in addition to the damping from η.

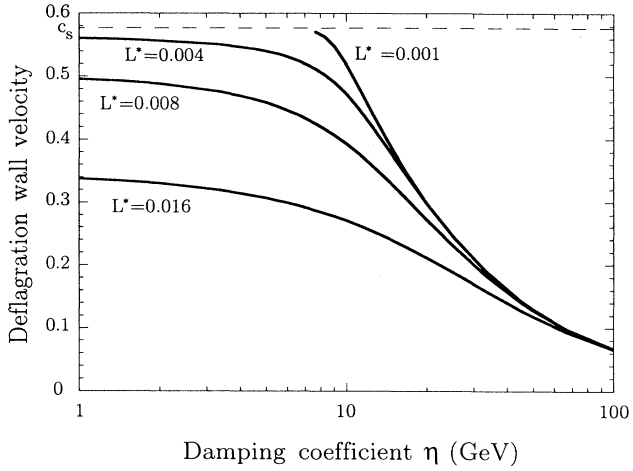

FIG. 3. Deflagration wall velocity v_0 as a function of the damping coefficient η. The velocity is calculated with several different values of the latent heat parameter $L^* \equiv L/(3aT_c^4)$. Unless otherwise stated, in Figs. 3–6 the parameters take the values $L^* = 0.004$, $\sigma = 0.005T_c^3$, $\xi = 15/T_c$, and $T_c = 100$ GeV. These values are close to the one-loop calculated values; see Eq. (17). Some of the lines in the figures stop. For example, the $L^* = 0.001$ line stops where $v_0 \approx c_s$ because our approximation (43) breaks down. One might expect that the wall becomes a detonation at the point [3]. Note that EW theory predicts that $\eta \sim g_W^2 T_c \sim 30$ GeV [see Eq. (28)]. For a wide range a parameter space, this puts $v_{\rm def}$ well below c_s.

down the bubble walls because the greater heat released will raise T_b and T_u. Note also that most of the released latent heat is transported in front of the bubble wall (remember these are spherical bubbles with r^3 dependence on volume). We will use this fact later.

Figures 3–6 show the main results of this section: the deflagration wall velocity as a function of η for various values of the EW parameters. The main point of these graphs is that there is a wide range of parameter space that produces deflagration wall fronts. Recall that we estimated the actual value of η to be of order $\eta \sim g_W^2 T_c \approx 0.3T_c$ (see Sec. IV B).

One of the most interesting characteristics of Figs. 3–6 is that v_0 *does not increase linearly with* η^{-1}, as one might naively expect from Eq. (33). That is to say, the wall velocity depends not only on the damping coefficient η, but also on how quickly heat can be transported away from the wall, because the pressure difference across the wall is temperature dependent. [Recall this was briefly discussed in the arguments following Eq. (25).] This process is what one might call the "shark-fin effect" (see Fig. 2): The faster the deflagration wall goes, the higher the temperature of the plasma around the wall and the more the wall resists going even faster. This effectively acts as kind of hydrodynamical damping on the bubble wall, which is in addition to damping due to internal bubble wall mechanics. Ultimately, this damping will be limited by heat conduction, which is not included in these calculations because the transport of heat due to diffusion is much smaller (in our case) than the transport of heat from the bulk flows and shock calculated above.

One should always keep in mind that in these calculations we have made several assumptions. For example, we have parametrized the wall thickness with the factor n_w. As stated before, the above calculations use $n_w = 2$ because this is its value when damping and thermal diffusion are neglected. If anything, one would expect $n_w \gtrsim 2$ because of damping and thermal diffusion. To a first approximation, inspection of (33) tells us that changing n_w is effectively changing η. Therefore one can get an idea of

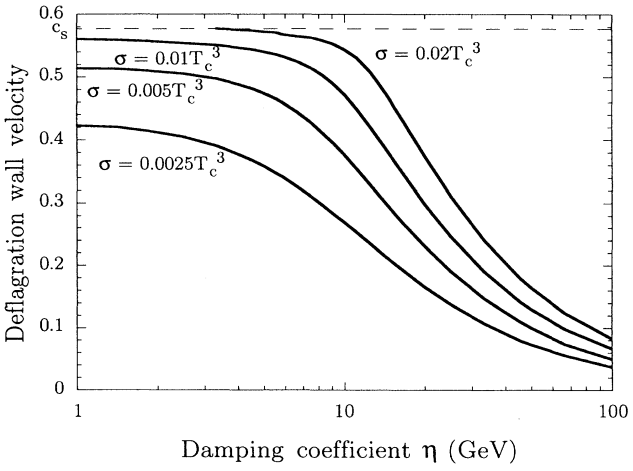

FIG. 4. Same as Fig. 3, but with several values of the bubble wall surface tension σ.

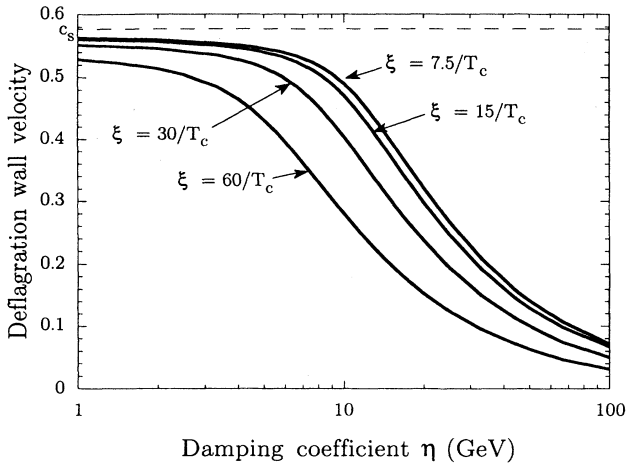

FIG. 5. Same as Fig. 3, but with several values of the Higgs correlation length ξ.

how changing n_w will change v_0 by looking at Figs. 3–6 and changing η accordingly.

Another approximation was used with the assumed temperature profile of the bubble wall (3). As stated before, full numerical calculations show that the shape of $T(x)$ is different than (3) and there may also be a shift with respect to $\phi(x)$ [3]. These numerical calculations, which only use conservation of energy and momentum, show that the temperature profile is shifted toward the b phase. One would also expect that some heat would thermally diffuse into the b region because it is at a lower temperature than the u phase at the wall (see Fig. 2). We have performed calculations including a shift in $T(x)$ with respect to $\phi(x)$ of the form

$$T(x) = \frac{T_u + T_b}{2} + \frac{T_u - T_b}{2}\left(1 - 2\frac{\phi(x+\epsilon)}{\phi_b}\right), \quad (45)$$

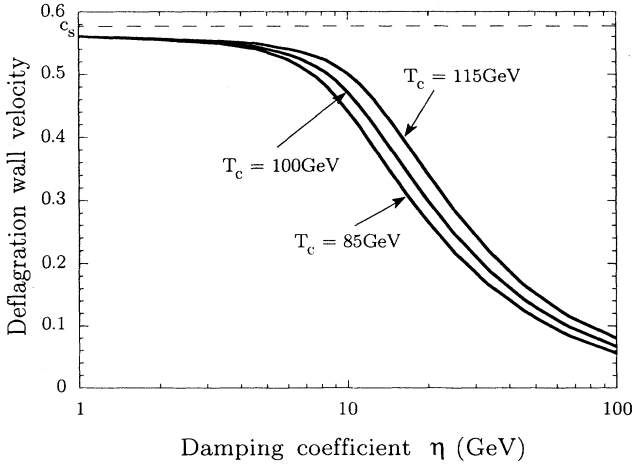

FIG. 6. Same as Fig. 3, but with several values of the critical temperature T_c.

where ϵ is the shift, and we have found that a shift in the direction of the b phase ($\epsilon > 0$) only *decreases* the velocity of the deflagration front. In fact, a shift on the order of a correlation length only decreases v_0 by about 10–20%. A shift in the opposite direction will increase v_0 ($\epsilon \approx -\xi$ can increase v_0 by as much as a factor of 2), but the above-mentioned numerical calculations and thermal diffusion make this shift unrealistic. Therefore we can have some confidence that these changes will not qualitatively effect our results that are based on assuming the wall is a deflagration.

V. THREE SCENARIOS OF THE PHASE TRANSITION

The dynamics of the phase transition depend on the velocity v_0 of the bubble walls before the bubbles begin to influence each other. The behavior of the transition can be separated into three classes: $v_0 \geq c_s \equiv 1/\sqrt{3}$, $v_0 \lesssim c_s$, and $v_0 \ll c_s$. Figure 7 presents a qualitative description of the three cases.

A. Case 1: $v_0 \geq c_s$

This is the easiest scenario to calculate. Since v_0 is greater than the speed of sound, it has been shown that the bubble wall must propagate as a detonation [22,24]. Since no latent heat is transmitted in front of the bubble wall for detonations (see Fig. 7), the bubble walls cannot influence each other until they actually collide. There-

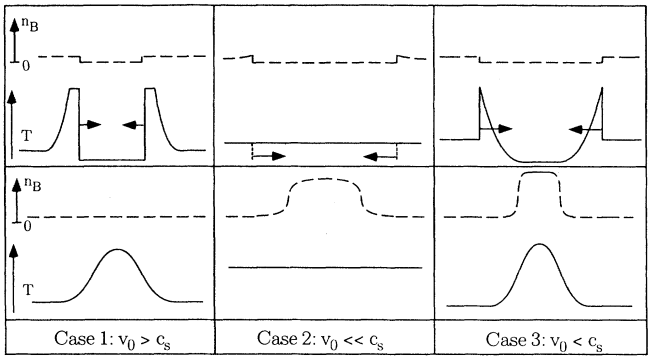

FIG. 7. Qualitative picture of the three possible scenarios of the phase transition. For case 1, the wave is a detonation (though, strictly speaking, for spherical symmetry, there is no constant temperature region in the wave). For cases 2 and 3, the wave is a deflagration. The top three boxes are snapshots of the phase transition for each case just before the bubble walls collide. The arrows begin at the wall fronts and indicate which direction the walls are propagating. The bottom three boxes are snapshots just moments after the bubble walls have collided. Each box includes a qualitative temperature and baryon density profile. Note that in case 2 the temperature is homogeneous, and the bubble wall front is indicated with a dashed line. Note also that since all temperature fluctuations are much smaller than T_c, their affect on baryon density is negligible.

fore the velocity of the bubble walls is unaffected by the presence of other bubbles and $v(t) = v_0$. In this case, there is no baryon enhancement, $\chi = 1$, and the baryon density is homogeneous.

Small inhomogeneities may have been produced at the wall collisions, but the size of these inhomogeneities $\sim$ bubble wall width. These inhomogeneities are so small that they would be quickly erased by thermal diffusion.

B. Case 2: $v_0 \ll c_s$

When v_0 is less than the speed of sound, the bubble wall propagates as a deflagration [22,29]. One main characteristic of a deflagration front is that a shock front precedes it, with a velocity $v_{sh} > c_s$. This means that some of the latent heat is transmitted far in front of the deflagration wall, and this reheated plasma will influence neighboring bubbles. In fact, if v_0 is small enough, one can assume that the latent heat released has been uniformly distributed throughout space. This is the limit of case 2: We will assume that all of the latent heat released by the bubble wall has ample time to completely equilibrate, and the temperature T is the same everywhere in space.

In this case, since $T = T_u = T_b$, we can use Eq. (34) to define $v(t)$. That is, in the small velocity limit,

$$v(t) = \frac{n_w \xi}{8\eta\lambda}\left[3B^2T(t)^2\left(1 - \frac{\sqrt{B^2T(t)^2 + 8(\lambda A - B^2)[T_c^2 - T(t)^2]}}{BT(t)}\right) + 12(\lambda A - B^2)[T_c^2 - T(t)^2]\right] . \quad (46)$$

Now our problem is reduced to finding $T(t)$, the temperature as a function of time. This can be done by using the conservation of energy in the following way.

The pressure p and energy density ρ for the high- (u) and low- (b) temperature phases are defined by

$$p_b(T) = aT^4 + V(T), \quad p_u(T) = aT^4 ,$$
$$\rho_b(T) = 3aT^4 + TV'(T) - V(T), \quad \rho_u(T) = 3aT^4 , \quad (47)$$

where $a \equiv (\pi^2/90)N$, $N = 106.75$ is the number of degrees of freedom of the plasma at $T \simeq 100$ GeV [30], and $V(T)$ is defined as the minimum of $V(\phi, T)$. In order to find $T(t)$, let us first ignore the expansion of space (we will add it back shortly). Consider a volume V_0 of space initially in the u phase and at some temperature $T_n < T_c$. Bubbles will be nucleating and growing in this volume, and the latent heat released will reheat the plasma in such a way that the total energy in V_0 will be conserved:

$$\rho_u(T(t))F(t) + \rho_b(T(t))[1 - F(t)] = \rho_u(T_n) . \quad (48)$$

If we now take the time derivative of both sides of this equation, it can be shown, either numerically or by using the simple approximation [30] $V(T) \simeq L/4(1 - T^4/T_c^4)$, that the second derivative term (d^2V/dT^2) is negligible, and Eq. (48) becomes

$$\left.\frac{dT}{dt}\right|_{\text{reheat}} = \frac{1}{12aT^3}\left(T\frac{\partial V(T)}{\partial T} - V(T)\right)\frac{dF(t)}{dt} . \quad (49)$$

The effect of the expansion of the Universe is to decrease the energy density, and so we need to add a term to Eq. (49) to account for this. When the Universe is not undergoing a change in its equation of state, the temperature obeys the relation

$$\left.\frac{dT}{dt}\right|_{\text{expansion}} = -TH(T) , \quad (50)$$

where $H(T) \equiv \sqrt{8\pi\rho(T)/3m_{\text{Pl}}^2}$ is the inverse Hubble time and m_{Pl} is the Planck mass.

Putting Eqs. (49) and (50) together, we obtain a formula for the evolution of the temperature as a function of time:

$$\frac{dT}{dt} = \frac{1}{12aT^3}\left(T\frac{\partial V(T)}{\partial T} - V(T)\right)\frac{dF(t)}{dt} - T\left(\frac{8\pi(3aT^4)}{3m_{\text{Pl}}^2}\right)^{1/2} . \quad (51)$$

Substituting in the expressions for $F(t)$, $V(T)$, and $v(T(t))$, we find that (51) is an integro-differential equation which must be solved numerically. Once $T(t)$ is known, however, one can easily calculate $v(t)$ and the baryon enhancement factor χ.

The amplitude and size of baryon density inhomogeneities can also be calculated. As the bubbles grow, they will heat up the plasma and slow down. Since we know that the baryon density $n_B \sim v(t)^{-1}$, we can calculate the baryon density profile the bubble wall leaves behind as it propagates through space. That is to say, we can calculate the baryon over density $\delta_B(r)$ defined as

$$\delta_B(r) \equiv \frac{n_B(r)}{n_{B0}} = \frac{v_0}{v(r)} , \quad (52)$$

where n_{B0} is the baryon density assuming the wall velocity is constant ($v = v_0$), and knowing $v(t)$ at all times allows us to find the velocity as a function of bubble radius r.

One must be careful, however, in using (52), because the bubbles are nucleating randomly in space, and so the

distance a bubble wall propagates before colliding with another is not well defined. We can get a good idea of the general behavior and scale by using the average bubble spacing

$$d(t) = (n_{\rm bubl})^{-1/3} = \left(\int_{t_c}^{t} \Gamma_{\rm nuc} dt \right)^{-1/3} . \quad (53)$$

Therefore d is the scale size for inhomogeneities and $\delta_B(r)$ only has meaning out to scales of this order. For the EW phase transition, one typically finds that $d \sim 10^{-5} H^{-1}$.

Before moving on to the next case, let us make two remarks about this case. The first remark is actually a helpful rule of thumb. We have stated before that as the phase transition proceeds the released latent heat will reheat the plasma and the velocity of the walls will slow down. In order to get an idea of how important the reheating of the phase transition is, we can compare the latent heat L to the energy needed to bring the plasma back up to T_c from T_n. If

$$L < \rho(T_c) - \rho(T_n) = 3a(T_c^4 - T_n^4) , \quad (54)$$

then the latent heat will be too small to reheat the temperature back up to T_c. In this case, we would then expect that the bubble wall velocity will not slow down very much, and both χ and δ_B will be of order unity.

On the other hand, if

$$L \gtrsim 3a(T_c^4 - T_n^4) , \quad (55)$$

then the latent heat will reheat the plasma back up to T_c and the velocity of the bubble walls will slow down considerably. In this case, $\chi \gg 1$ and $\delta_B \gg 1$.

The second remark has to do with the case of large latent heat. If the plasma heats up enough, then the phase transition will almost stop. It will not stop completely, however, because the expansion of the Universe is continuously removing energy from the plasma, and so the temperature never quite reaches T_c. Instead, the temperature remains constant, while the released latent heat goes into expanding the Universe. We can use this fact to estimate the minimum velocity of the bubble wall by setting $dT/dt = 0$ in Eq. (51). If we now use the estimates $F \approx 0.5$, $TV'(T) - V(T) \approx L$, $\dot{F}/F = \dot{V}/V \approx 3v/r$, where r is the radius of an average bubble and $r \approx d/2$, we obtain an estimate for the minimum velocity:

$$v_{\rm min} \approx \frac{4dH}{(L/aT^4)} . \quad (56)$$

For the EW phase transition, we will find that $v_{\rm min}/v_0 \sim 1\text{–}10^{-3}$, which yields overdensities of $\delta_B^{\rm max} \sim 1\text{–}10^3$.

C. Case 3: $v_0 \lesssim c_s$

This is the most difficult case. Since $v_0 \lesssim c_s$ (but always $< c_s$), the bubble walls also propagate as deflagrations, as in case 2, and insofar as the deflagration picture is correct, this is also the most accurate description of the dynamics of the phase transition.

In this case, a shock front also precedes the deflagration front, but now the deflagration front is moving too quickly for the released latent heat to equilibrate with the rest of the plasma. Now there is a buildup of heat around the deflagration front and there is a temperature difference across it. The calculation becomes much more difficult because of the inhomogeneous distribution of temperature and the random distribution of bubbles.

Although a full numerical simulation is needed to accurately calculate the phase transition in this case, we produce a calculation in the Appendix which estimates the baryon enhancement χ and also the size and amplitude of the inhomogeneities produced. The results of this estimate are given in Sec. VI.

VI. NUMERICAL RESULTS

In this section, we will present and discuss numerical results of the EW phase transition for various values of the parameters of EW theory. The numerical calculations will be based on the limit of case 2, which assumes that the latent heat released during the phase transition is homogeneously (and instantaneously) distributed throughout space. We will also compare these results to approximations obtained for case 3.

The numerical calculation is done by evolving the phase transition in discrete time steps much shorter than the duration of the phase transition. As stated before, the relevant equation of evolution is (51).

A. Dynamics of the phase transition

Figure 8 shows the evolution of the temperature of the Universe, velocity of the bubble wall, and the fraction of space converted to the low-T phase during the transition for two values of the latent heat L. For large values of the latent heat, one can see that the phase transition quickly reheats the Universe close to T_c, and then the phase transition proceeds only because the Universe is expanding and removing the latent heat released.

A larger latent heat actually affects the phase transition in two ways. First, the larger the L, the more heat is released, and second, a larger L changes the shape of the potential $V(\phi, T)$ such that bubbles nucleate sooner. This decreases the temperature difference $T_c - T_n$ and makes any released latent heat that much more effective at reheating the plasma back up to T_c.

B. Baryon enhancement

Figure 9 shows the baryon enhancement χ as a function of L for different values of σ, assuming that $n_B \propto v_0^{-1}$, as predicted by charge transport mechanism (see Sec. II). Figure 9 is a calculation of χ for case 2, the case where the bubble wall velocity $v_0 \ll c_s$, and uniform reheating of the plasma is assumed. Our calculations show that, for

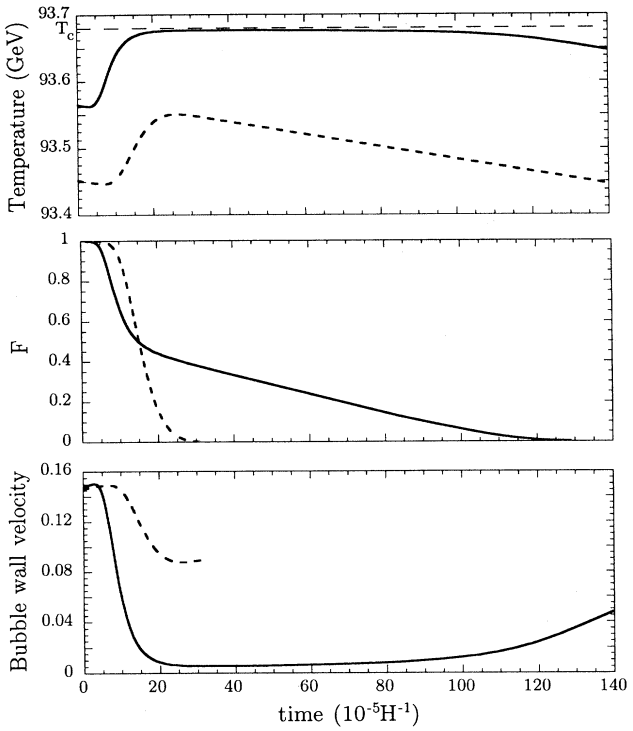

FIG. 8. Evolution of temperature, fraction F of unbroken phase remaining, and bubble wall velocity during the phase transition, as a function of time in units of $10^{-5}H^{-1}$, where H^{-1} is the inverse Hubble time. The solid line is for the case $L/(3aT_c^4) = 0.008$, and the dashed line is for the case $L/(3aT_c^4) = 0.004$. All of the other parameters are given the EW one-loop values ($\sigma = \sigma_0$, etc.). The initial time $t = 0$ is arbitrarily defined as the time when 10^{-6} of the Universe has converted to the low-temperature phase.

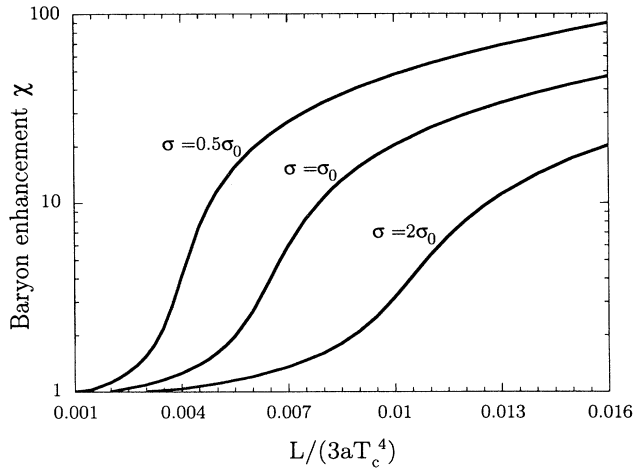

FIG. 9. Baryon enhancement factor χ as a function of latent heat parameter $L' \equiv L/(3aT_c^4)$ for various values of surface tension σ for the case of uniform heating (case 2). The quantity σ_0 is the one-loop EW theory value, defined in the text. All other values of the parameters are also the one-loop values. Here we use $\Gamma = 0.03/\text{GeV}$, though χ is relatively insensitive to Γ.

case 2, χ is relatively insensitive to the initial bubble wall velocity. This also translates into the fact that, for case 2, χ is relatively insensitive to the damping parameter η (of course, η must be large enough in order for case 2 to be a valid approximation).

For case 3, however, our estimate of χ can be a very sensitive function of the bubble wall velocity [see Eq. (68)], and so it can also be sensitive to η. (In Fig. 12, we have plotted χ as a function of η for several values of latent heat L in the limit of case 3.) Note, however, that as L increases, χ becomes less sensitive to η. As mentioned before [in the discussion after Eq. (68)], one must be careful in choosing the value d of the spacing between bubbles when calculating the case 3 estimate of χ. For Fig. 10, we have used the estimate that d is equal to the asymptotic value obtained from case 2. See the next section for a complete discussion of how d is obtained.

It is interesting to note in Fig. 10 that χ has a *maximum* value as η is varied. This can be explained by the fact that there are two competing effects: As the velocity increases from zero (i.e., damping increases), the size ℓ of the over dense regions becomes smaller, decreasing the average baryon density, but at the same time as the velocity increases, the minimum velocity of the bubble walls decreases, thus raising baryon production. At some point between small and large velocities, the combination of the two effects produces a maximum.

By comparing Figs. 9 and 10, we can compare the results of baryon enhancement χ for cases 2 and 3. First, let us recall that the case 3 estimate is only valid when the latent heat is large enough that Eq. (63) is satisfied. In Fig. 10, this constraint is satisfied for all values of η for the $l^* = 0.016$ and 0.008 curves, but for the $L^* = 0.004$ curve, the approximation is only valid for values $\eta \lesssim 10$ GeV. The values of χ for both cases are very similar (within $\sim 30\%$ of each other) for the two larger values of the latent heat.

There are two important observations to make from

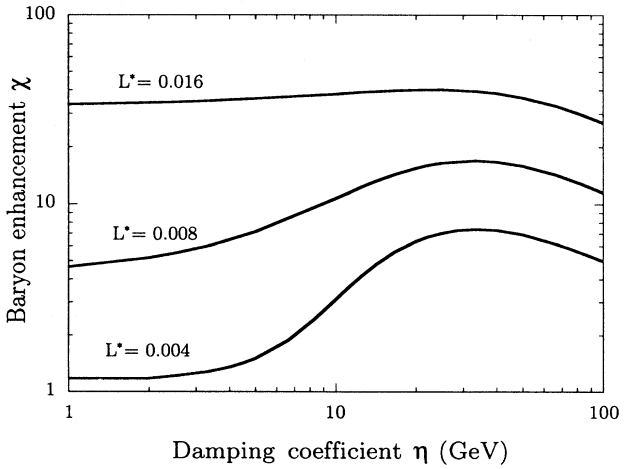

FIG. 10. Baryon enhancement factor χ as a function of the damping coefficient η for various values of latent heat L for the case of nonuniform heating (case 3). All other values of the parameters are also the one-loop values.

the comparison of these two figures. First, for small velocities (i.e., large damping), where case 2 is expected to be a good approximation, the two estimates of χ roughly agree. Second, for the difficult to (exactly) calculate scenario of larger bubble wall velocities, where inhomogeneous heating of the plasma becomes appreciable and case 3 becomes the valid estimate, we note that for larger velocities (smaller damping) χ decreases, though only by a factor of order unity. Therefore, instead of having to make the very complicated calculation of inhomogeneous heating, we estimate that the calculation of χ, assuming uniform heating of the plasma is a good approximation, and the effect of inhomogeneous heating only change the value of χ by a factor of order unity.

From Figs. 9 and 10, we can conclude that for baryon production inversely proportional to the wall velocity there is a wide range of parameter space that produces a large $\chi > 10$. Recall that a large χ relaxes constraints on other parameters such as CP violation.

Finally, note that χ can be a sensitive function of both L and σ for certain regions of parameter space. The one-loop EW value $L_0/3aT_c^4 \approx 0.004$ is within this sensitive region.

C. Inhomogeneities

For cases 2 and 3, which describe expanding deflagration bubbles, we have found that the bubble wall velocity decreases as the phase transition proceeds. This is a generic feature of cases 2 and 3. If one now assumes that baryon production is a function of bubble wall velocity, then inhomogeneities must develop during the phase transition.

In order to get an idea of the size and amplitude of the inhomogeneities produced, one can use the calculation of $v(t)$ obtained in the previous section on the dynamics of the phase transition to determine the velocity of the bubble wall as a function of bubble wall radius, i.e., $v(r)$. Then one can apply a velocity-dependent theory of baryon generation to obtain the baryon density as a function of radius from the bubble center, $n_B(r)$.

We must be careful, however, in interpreting the function $v(r)$, because our calculation of $v(r)$ assumes that the bubbles expand without colliding into other bubble deflagration walls. In reality, deflagration walls will collide on many scales as a result of not only the fact that the bubble centers are scattered randomly throughout space, but also because bubbles are continually nucleating during the phase transition. One can, however, sensibly talk about an *average* spacing between bubbles, $d(T)$ [see Eq. (53)], and we can then assume that the bubble walls propagate a distance $d(T)/2$ before colliding with other deflagration walls. This distance decreases with time, but as shown in Fig. 11, $d(T)$ reaches an asymptotic value during the phase transition. This is because at some point during the phase transition the released latent heat has reheated the plasma to a high enough temperature that nucleation has turned off, and so the distance between bubble centers remains constant (ignoring the very slow expansion of the Universe).

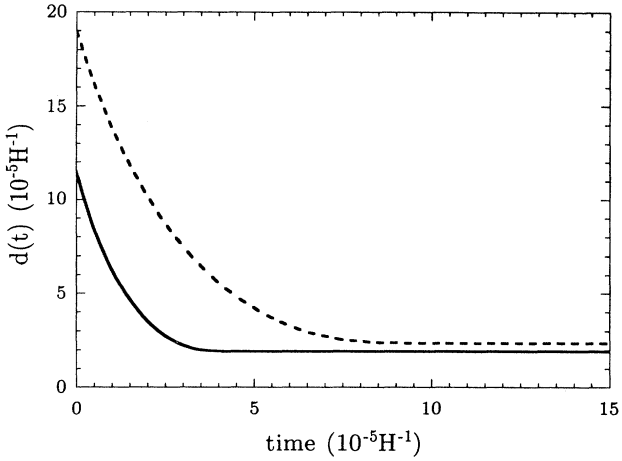

FIG. 11. Average spacing between bubble centers as a function of time for two different values of latent heat L. The notation and $t = 0$ in this figure is the same as in Fig. 8.

This asymptotic value for the distance between bubble centers d_0 sets the scale for the maximum size for the inhomogeneities. Figure 12 shows d_0 as a function of latent heat for various values of σ. We have found that since $d(T)$ is such a sensitive function of temperature, it reaches its asymptotic value as soon as the temperature begins to rise, which is very early in the phase transition (compare Figs. 8 and 11) for large enough values of latent heat. If L is so small that the temperature never rises during the phase transition, then $d(T)$ continues to decrease until the phase transition is complete.

Since the number density of bubbles $\approx d(T)^{-1/3}$, we can see by inspection of Fig. 11 that since $d(T)$ changes so rapidly, most of the bubbles are nucleated just before $d(T)$ reaches its constant value d_0 and nucleation turns off as a result of reheating. Therefore, since most of the bubbles are nucleated when the average spacing

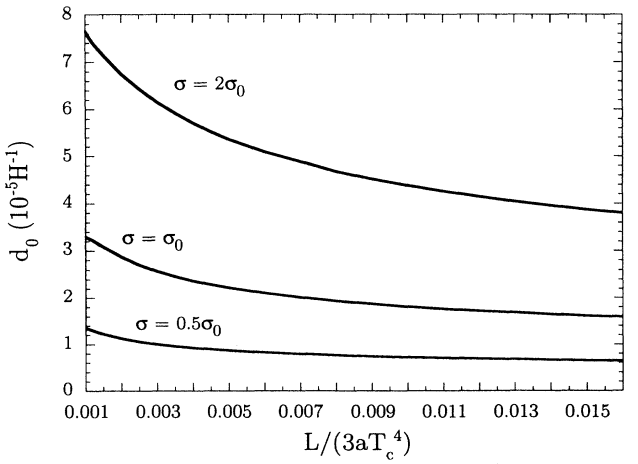

FIG. 12. Asymptotic value d_0 of the bubble center spacing as a function of latent heat for various values of σ.

between bubble centers is constant (d_0), we can sensibly talk about bubbles propagating a distance $d_0/2$ before colliding with other deflagration walls, and we then have a reasonable interpretation of the calculation of $v(r)$. In Fig. 13, we have plotted $v(r)$ for a bubble nucleated at the peak nucleation time, i.e., the time when the bubble nucleation rate is the largest or, put another way, the time at which $\partial n_{\rm bubble}(t)/\partial t = 0$, where $n_{\rm bubble}$ is the density of bubbles. For a large range of parameters, we found that, numerically, the peak nucleation time is at most a few $\times 10^{-5} H^{-1}$ before $d(T)$ reaches its constant value.

Not only the size, but also the amplitude of the inhomogeneities produced can also be inferred from $v(r)$ (Fig. 13). One can see that the velocity of the bubble walls can decrease anywhere from a factor of order unity to a few orders of magnitude, depending on the values of parameters such as latent heat L or surface tension σ. In order to get a clearer idea of the range of velocities, we calculate the ratio $v_{\rm min}/v_0$, where $v_{\rm min}$ is the minimum velocity the wall acquires during the phase transition. We present the result of $v_{\rm min}/v_0$ as a function of latent heat L for various values of σ in Fig. 14. If the amplitude of inhomogeneities $\delta_B \sim v^{-1}$ [see Eq. (52)], then Fig. 14 is also a graph of $(\delta_B^{\rm max})^{-1}$.

In order to determine the density profile for the case when baryon production is inversely proportional to the bubble wall velocity, as the charge transport mechanism predicts (see Sec. II), we have plotted $v_0/v(r)$ in Fig. 15 (also nucleated at peak nucleation time as defined above) for two different values of the latent heat, where r is the distance from the bubble center and v_0 is the bubble wall velocity before other bubbles affect the velocity. On this graph, we have also plotted the average baryon density. Note that for this case the inhomogeneities are characterized as large regions of baryon density, which is slightly more dense than the average (by a factor of at most a few), along with large *holes* of very low density of baryons (smaller than the average by up to a few orders of magnitude). This type of baryon density profile, i.e., one with holes of almost zero density, is the opposite of the type of density profiles normally considered for inhomogeneities in the early Universe, namely, small regions

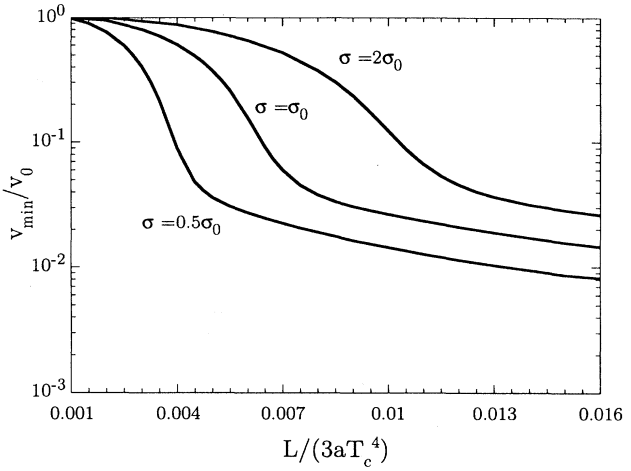

FIG. 14. Minimum velocity (divided by the initial velocity) that a bubble wall acquires during the phase transition for case 2 as a function of latent heat L and for various values of σ.

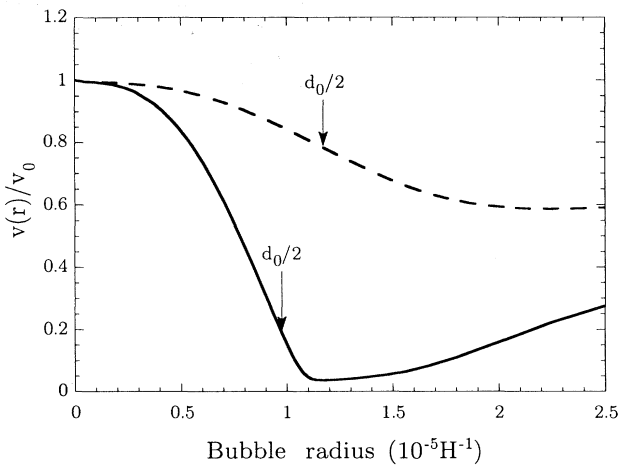

FIG. 13. Plot $v(r)/v_0$ for $L/(3aT_c^4) = 0.008$ (solid line) and for $L/(3aT_c^4) = 0.004$ (dashed line), where $v(r)$ is the bubble wall velocity, r is the bubble radius, and v_0 is the initial bubble wall velocity. We have indicated the radius $d_0/2$ at which the bubbles will, on average, collide. Note that if baryon production is proportional to the wall velocity, then this is also a plot of the density profile as a function of distance r from the bubble center.

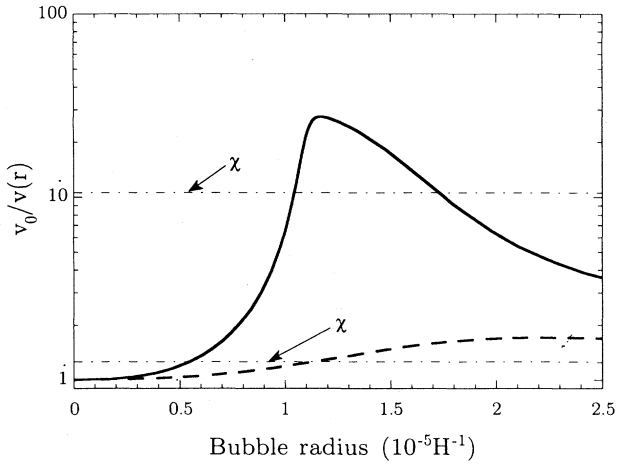

FIG. 15. Plot $v_0/v(r)$ for $L/(3aT_c^4) = 0.008$ (solid line) and for $L/(3aT_c^4) = 0.004$ (dashed line), where $v(r)$ is the bubble wall velocity, r is the bubble radius, and v_0 is the initial bubble wall velocity. For baryon production proportional to the inverse bubble wall velocity, this is also the baryon density profile of the bubble. We have also plotted the baryon enhancement χ for both cases [e.g., the upper dot-dashed line is for the $L/(3aT_c^4) = 0.008$ case] because in these units, normalized by v_0, χ is the average baryon density.

with large baryon over density surrounded by regions of baryon density close to the average. We will talk more about these different types of profiles in the next section.

So far in this section we have only talked about inhomogeneities generated for case 2, where the heating is homogeneous. For case 1, as we have discussed before, no significant inhomogeneities are expected to form at all. But what about case 3, the most realistic deflagration wall scenario? As stated in the previous section, case 3 evolves in a way very very similar to case 2. The inhomogeneities generated should also be similar. The only difference between cases 2 and 3 is that for case 3 the size of the inhomogeneities will be smaller and their amplitude larger.

The size of the inhomogeneities for case 3 will be ℓ [see Eq. (A4)], which is always smaller than $d_0/2$, the size of inhomogeneities for case 2. We should make it clear here that the *separation* between the inhomogeneities will be the average bubble spacing $\approx d_0$ for both cases, though the physical *size* of the inhomogeneities is different for each case. Since the minimum velocity attained is smaller in case 3, one might expect that the amplitude of the inhomogeneities for case 3 will be larger than in case 2 [see Eqs. (A5) and (A6)]. How much smaller in size and larger in amplitude the inhomogeneities will be for case 3 compared to case 2 depends on how close the bubble wall velocity is to the speed of sound, c_s (because the closer to c_s the more concentrated is the released latent heat). For the one-loop EW parameters (and assuming $\eta = 0.3T_c$), for example, $v_{\min} \approx 0.14$, and the difference between cases 2 and 3 is that the amplitude of the inhomogeneities is only 1.6 times greater for case 3 and the size is 1.6 times smaller, assuming that baryon production $\sim v_0^{-1}$.

As a final note, although we have shown that the velocity of the bubble wall can vary by as much as a few orders of magnitude, we stress that how this translates into inhomogeneous baryon production depends on the model of baryogenesis. For weak dependence of velocity on baryon production, this several magnitude variation in v_0 would only produce small amplitude inhomogeneities. However, as shown in Sec. II, there could be *very* strong dependence (exponential) of velocity on baryon production, and this could produce very large amplitude inhomogeneities. In fact, one might imagine that in the exponential dependence regime the production of very dense inhomogeneities could form objects that may even collapse onto black holes. The v_0^{-1} dependence that we have chosen to use as the main example in this paper produces moderately large amplitude inhomogeneities.

VII. EFFECTS ON PRIMORDIAL NUCLEOSYNTHESIS

Now that we have determined the size and amplitude of the inhomogeneities generated in the phase transition for various scenarios, let us examine whether these inhomogeneities will have any observable effects on the production of elements in the early Universe. We will see that the crucial factor that will determine whether the inhomogeneities have any effect on the production of elements will be their ability to survive the homogenizing effects of diffusion.

The standard calculation of big bang nucleosynthesis (BBN) predicts element abundances that are consistent with observational constraints (e.g., see [32]). This calculation assumes that the Universe was homogeneous at the time of nucleosynthesis. There are, however, BBN calculations that include the presence of inhomogeneities during nucleosynthesis (for example, see [33,34]), and these calculations produce abundances significantly different than the homogeneous case.

The important result of these inhomogeneous BBN calculations is that there is a large range of sizes and amplitudes of inhomogeneities that can be *ruled out* because they produce abundances that do not agree with observation [34]. So the important question is, does any region of EW parameter space produce inhomogeneities that are ruled out by observations of primordial element abundances? In order to answer this question, we must first determine what these inhomogeneities, which were formed early on when the temperature of the Universe was $\sim$ 100 GeV, look like much later, when nucleosynthesis takes place, at a temperature $\sim$ 100 keV.

A. Evolution of the inhomogeneities up to the nucleosynthesis epoch

Once the inhomogeneities are formed in the plasma, they will immediately begin to dissipate via diffusion. The time scale for complete dissipation of the inhomogeneity will depend upon the size and amplitude of the inhomogeneity, and it will also depend upon the mean free path of the particles responsible for the diffusion. In the early universe, there are many different kinds of particles in the plasma, but it is the particles with the largest mean free path (though so large that they become decoupled from the plasma) that play the dominant role in diffusion. For example, for a temperature T in the range 100 GeV $< T <$ 1 MeV, neutrinos have the longest mean free path, and they are responsible for the dissipation of the inhomogeneities [35,36]. As the temperature decreases, however, neutrinos decouple from the plasma, and then the baryons and eventually photons become the dominant diffusing particles [36].

In order to have an effect on nucleosynthesis, any baryon density inhomogeneities generated in the EW phase transition must survive until the nucleosynthesis epoch. If the inhomogeneities are too small in size (and, strictly speaking, amplitude), they will be dissipated by diffusive processes and will have no effect. One can therefore place a lower limit on the size of inhomogeneities, below which there are no observable effects on the abundances of the elements. In order to find this lower limit and ultimately if the EW phase transition generates inhomogeneities larger than this lower limit, let us look closer at the neutrino, baryon, and photon diffusion processes.

Heckler and Hogan [35] and Jedamzik and Fuller [36] have studied the dissipation of inhomogeneities due to neutrino diffusion, and they have found that a wide range of sizes and amplitudes can easily survive until 1

MeV, when other diffusive processes become important. In particular, for the scales sizes $d_0 \approx 10^{-5}H^{-1}$ ($T = 100$ GeV) $\approx 10^{-6}$ cm, typical for the EW phase transition, neutrino diffusion will not significantly affect inhomogeneities with amplitudes smaller than $\sim 10^4$, and amplitudes larger than this would simply decrease until they reached 10^4. Put another way, neutrino diffusion will have a negligible affect on the inhomogeneities generated in the EW phase transition.

Therefore the important processes that significantly dissipate the inhomogeneities generated in the EW phase transition are baryon and photon diffusion. Jedamzik and Fuller [36] have shown that, for temperatures well into the nucleosynthesis epoch, baryon diffusion dominates over photon diffusion. Photon diffusion does play a significant role in the dissipation of the inhomogeneities for later times in the nucleosynthesis epoch, but in order to obtain an (optimistic) estimate of the survival of the inhomogeneities at the nucleosynthesis epoch, we will neglect photon diffusion and concentrate on baryon diffusion only.

The important scales for determining the effect of baryon diffusion are the proton diffusion length and the neutron diffusion length. The diffusion length of a particle is defined as the average distance the particle will travel as it randomly walks through a plasma for some time t. Here the time t is the time from the initial creation of the inhomogeneity at the EW phase transition up to the nucleosynthesis epoch. Since the neutrons have no electric charge, they will have a much larger diffusion length than the protons, and they will diffuse out of baryon overdensities much quicker than the protons (see, e.g., [36]).

Therefore, since the protons diffuse slower than the neutrons, the proton diffusion length will be the limiting length scale for the dissipation of inhomogeneities. That is to say, if the inhomogeneities are much smaller than the proton diffusion length d_p, then they will dissipate before they can have any effect on nucleosynthesis.

Fuller *et al.* [37] have calculated the proton diffusion length integrated from the EW phase transition up to the beginning of the nucleosynthesis epoch. They have found that, for inhomogeneities with amplitudes less than 10^2, the proton diffusion length is

$$d^p_{100} \approx 0.1 \text{ cm} , \tag{57}$$

where d^p_{100} stands for the proton diffusion length comoving at 100 GeV. For inhomogeneities with amplitudes larger than 10^2, the comoving diffusion length decreases. For example, for an amplitude of 10^4, $d^p_{100} \approx 0.01$ cm (see Fig. 16).

How do these values compare with the typical length scale d_0 for the inhomogeneities generated in the EW phase transition? As seen from the previous section, the typical length scale for the inhomogeneities is $d_0 \sim 10^{-5}H^{-1} \approx 10^{-6}$ cm. In fact, for a wide range of parameter space,

$$\frac{d_0}{d^p_{100}} \approx 10^{-5} \ll 1 . \tag{58}$$

Therefore, if inhomogeneities are generated on the scale of d_0 and have amplitudes $\lesssim 10^{-4}$, they will all dissipate before they can effect nucleosynthesis.

Figure 16 presents d^p_{100} as a function of amplitude (obtained directly from Fuller *et al.* [37]). Also plotted in this figure are values of the average spacing between bubble centers d_0 (for various values of latent heat L and bubble surface tension σ), which is assumed to be the scale size for inhomogeneities generated in the EW phase transition. The amplitude of the inhomogeneities for these points was obtained by assuming that baryon generation is inversely proportional to bubble wall velocity, as predicted by the charge transport mechanism of baryogenesis. This figure illustrates very well that d_0 is much smaller than d^p_{100} for a large range of parameter space.

In order to get a more general idea of the size of the inhomogeneities produced in the EW phase transition, we have also plotted the mass and overdensity of the inhomogeneities in Fig. 17 and compared these with the masses and overdensities for which proton and neutrino diffusion is important. Note that the inhomogeneities generated are about 10^{-30} solar masses in size, and so we can see that in terms of the Universe today these inhomogeneities are very small in scale.

B. Possibilities for generating larger inhomogeneities

We have seen in the last section that the average spacing between bubbles, d_0, is much smaller than the comoving proton diffusion length, and if inhomogeneities

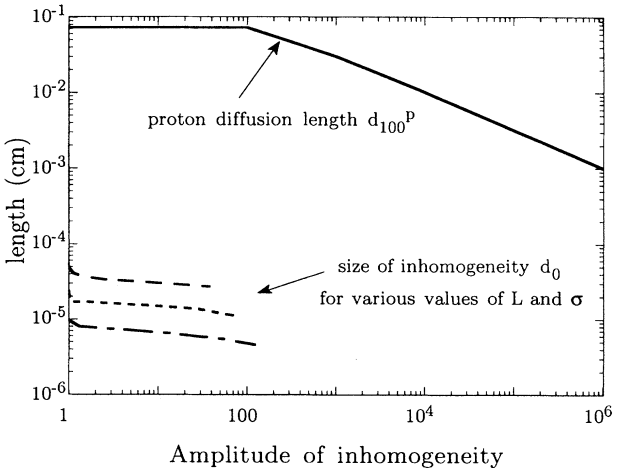

FIG. 16. Proton diffusion length d^p_{100}, comoving at 100 GeV, as a function of amplitude of inhomogeneity. These values of d^p_{100} are approximate, and they are taken directly from Fuller *et al.* [37]. We have also plotted lines which indicate the size d_0 and amplitude of inhomogeneities generated in the EW phase transition for various values of latent heat L and bubble surface tension σ. Each line represents a line of constant σ. $\sigma = 2\sigma_0$ (long-dashed line), $\sigma = \sigma_0$ (short-dashed line), and $\sigma = 0.5\sigma_0$ (dot-dashed line). The lines run from $L/(3aT_c^4) = 0.001$ to $L/(3aT_c^4) = 0.016$ from left to right. Note that for any of these values $d_0 \ll d^p_{100}$.

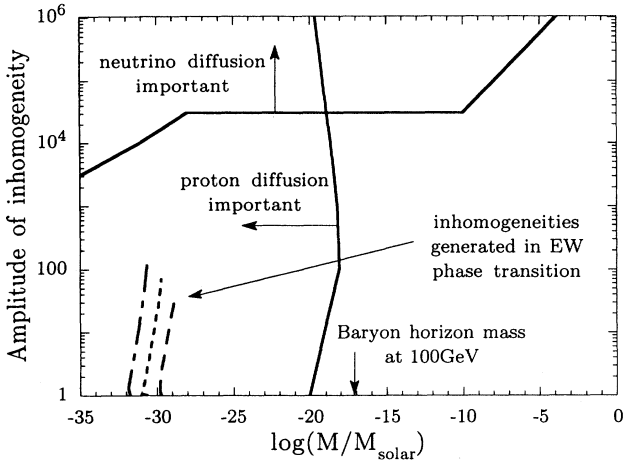

FIG. 17. Mass scale of inhomogeneities produced in the EW phase transition (with the same notation and data as in Fig. 16), compared with mass and overdensity scales for which proton and neutrino diffusions are important. The neutrino diffusion scales were taken directly from Jedamzik and Fuller [36].

are produced at this scale, they will dissipate before they can effect nucleosynthesis. However, if inhomogeneities are somehow generated on scales a few orders of magnitude larger than d_0 (depending on the amplitude of the fluctuations), then they would be able to survive until the nucleosynthesis epoch and affect the abundances of the elements. Below, we examine a plausible scenario for producing inhomogeneities on scales much larger than d_0 [38].

For example, consider the following plausible scenario for producing inhomogeneities much larger than d_0. From our observations of many known phase transitions (such as liquid boiling), we find that it is very common for phase transitions to be induced by "impurities" in the system, long before thermal nucleation has a chance to play a role. Let us apply this idea to the EW phase transition: What if bubble nucleation in the EW phase transition was induced by some impurity or seed, rather than by thermal nucleation?

First of all, if the phase transition was induced by a seed, the bubbles would be nucleated at a temperature much closer to T_c than if it was induced by thermal nucleation. Any latent heat released from the nucleated bubbles would therefore be much more effective at reheating the plasma back up to T_c, where nucleation ceases. If the plasma was reheated quickly back up to T_c and further bubble nucleation was turned off, one would expect that the scale size for inhomogeneities would now be the average bubble spacing at the time when nucleation turned off, just as in the thermal nucleation case. But in the seed nucleation case, the scale for average spacing between bubbles now depends the scale $d_{\rm seed}$ associated with the density (and efficiency of nucleation) of the seeding agent.

Even though we can only speculate on what the value of $d_{\rm seed}$ could be, we can still place an upper limit on the largest spacing between bubbles in the seed nucleation scenario, independent of $d_{\rm seed}$. This can be done by observing that, although it is true that the seed nucleated bubbles can reheat the Universe back up to T_c, it will still take a finite amount of time to do so, because the shocks carrying the released latent heat (we are assuming the bubble walls are deflagrations) can only travel at a speed $v_{\rm sh} < c$. If the shocks take too long to heat up the Universe, thermal nucleation will start to become important, and more bubbles will start to nucleate, decreasing the average spacing. The maximum amount of time $t_{\rm max}$ that the shock waves can have to reheat the plasma before thermal nucleation becomes important can be estimated as

$$t_{\rm max} \approx t(T_n) - t(T_c) \ , \tag{59}$$

where $t(T)$ is defined as the time at which the Universe is at a temperature T and T_n is the temperature at which the maximum number of bubbles is thermally nucleated (see Sec. VI C). This time can be translated into a distance $d_{\rm max}$. If we approximate $v_{\rm sh} \approx 1$, we find that, for a wide range of EW parameter space,

$$d_{\rm max} \approx 10^{-3} H^{-1} \approx 10^{-3} \text{ cm} \ , \tag{60}$$

where H^{-1} is the Hubble length at $T \approx 100$ GeV. Note that this is about two orders of magnitude bigger than d_0. However, this is still smaller than the proton diffusion length (see Fig. 16).

There is still the scale size $d_{\rm seed}$ to consider. For example, if there is some large scale coherence $d_{\rm seed}$ on the scale of a Hubble length associated with the seeding agent, then this would also produce inhomogeneities. Let us use an example. One possible seeding agent in the EW phase transition is cosmic strings [39]. If the density of these strings varied on scales comparable to the Hubble length, then one would expect that the amount of bubble seeding would also vary on the scale of a Hubble length. Regions with a large density of strings would nucleate very close to T_c, and as described above, these regions would also reheat quickly, and the bubble walls would quickly slow down. On the other hand, regions with low string density will nucleate at temperatures much farther away from T_c, and these regions would not reheat so quickly. The bubble walls in these low-density string regions would then propagate faster, because the temperature is farther away from T_c. Since the average bubble wall velocities are different in these two regions, one would expect that the baryon density would be different, and the scale size for these regions would be $d_{\rm seed}$.

To summarize, it is plausible that the seed nucleation scenario (caused, for example, by the presence of cosmic strings) could provide two scales for producing inhomogeneities: $d_{\rm max}$ and $d_{\rm seed}$. We have shown that although $d_{\rm max}$ is larger than the expected size for inhomogeneities generated via thermal nucleation, it is still much smaller than the proton diffusion length, and so they will not survive to effect nucleosynthesis. However, the seed nucleation scenario can also produce inhomogeneities on the scale $d_{\rm seed}$, which can be larger than the proton diffusion length, though the actual size of $d_{\rm seed}$ is presently still speculation.

VIII. CONCLUSION

The main conclusion of this paper is that phase transition dynamics can play an important role in electroweak baryogenesis. We have shown that through the course of the phase transition the bubble wall velocity can slow down by as much as a few orders of magnitude, depending on the values of the presently unknown parameters of the EW phase transition such as latent heat and bubble wall surface tension. Since all baryon production mechanisms are sensitive to bubble wall velocity for at least some range of velocities, the dramatic decrease in bubble wall velocity can change the average baryon density a few orders of magnitude from what is expected from calculations which assume that the bubble wall velocity is constant. In fact, we calculated baryon production in the EW phase transition using the model called the "charge transport mechanism," and we found that the average baryon density could be as much as 10^2 greater than the constant bubble wall velocity calculation. This enhancement of baryon production could ease the constraints (from the observed average baryon density) on other parameters of the theory, such as the amount of required CP violation.

In addition to affecting the average baryon density, the changing bubble wall velocity also produces inhomogeneities. The amplitude of the inhomogeneities depends upon the dominant mechanism of baryogenesis. For the charge transport mechanism, we found amplitudes as great as 10^2. The physical size of the inhomogeneities is a relatively insensitive function of the parameters of the EW phase transition, and we found that the characteristic scale size for inhomogeneities is $\approx 10^{-5}H^{-1}$, where H^{-1} is the Hubble length at the phase transition. These inhomogeneities are too small to survive until the nucleosynthesis epoch and affect the abundances of the elements. Instead, they dissipate via baryon diffusion before nucleosynthesis begins. There are, however, plausible (though speculative) scenarios that can produce large enough inhomogeneities that would affect nucleosynthesis. For example, if bubbles are nucleated by some seed such as cosmic strings, then the string density scale may be large enough to create large inhomogeneities.

Besides the topic of baryogenesis, we have also made some interesting conclusions about bubble wall propagation in the EW phase transition. Most notably, we have found that for a very wide range of parameter space the bubble walls travel as deflagrations. There is not only "frictional" damping on the wall, which we parametrized with a damping parameter η, but we have also found that with the inclusion of the conservation of energy and momentum there is an additional "hydrodynamical" damping on the wall which is important, especially when the frictional damping η is small. The consequence of this hydrodynamical damping is to lower the bubble wall velocity to a point that all but the most weakly damped walls travel as deflagrations. It is important to show that the walls travel as deflagrations because it is only this type of bubble wall propagation (i.e., one with a shock that precedes it) that produces the interesting behavior of dramatic bubble wall deceleration due to reheating.

ACKNOWLEDGMENTS

The author would like to thank Peter Arnold, Larry Yaffe and especially Craig Hogan for many helpful comments and discussions. This work was supported by NASA Grants Nos. NAGW 2569 and NAGW 2523 at the University of Washington.

APPENDIX: ESTIMATING BARYON PRODUCTION IN CASE 3: $v_0 \lesssim c_s$

As stated before, the complexity of the phase transition prohibits any accurate calculations without a full numerical simulation. For example, in this case we have bubbles with shocks and complicated temperature profiles colliding with each other. Kajantie and Kurki-Suonio [2] and Ignatius *et al.* [3] have studied collisions of deflagration fronts and shock fronts in 1+1 dimensions, but in 3+1 dimensions, approximations similar to case 2 must be made if numerical simulations are not used (e.g., see [31]).

Since we are not using a numerical simulation, we will forego any detailed calculations and make some general arguments that will give us a good idea of what is happening during the phase transition in case 3. We will be able to estimate the baryon enhancement χ and the size and the overdensity δ_B of the inhomogeneities. We will find that case 3 is very similar to case 2.

The first idea to keep in mind is that case 2, which we can calculate, is a limit of case 3. Therefore one would expect that the behavior of the two cases should have some similarities. For example, in case 2 the bubble walls are continuously slowing down as a result of the reheating of the plasma as the growing bubbles homogeneously release their latent heat. The bubble walls in case 3 should also slow down as the phase transition proceeds, because the bubble walls are being influenced by the heated plasma of the shocks of neighboring bubbles.

Because the shock is so weak in the EW phase transition, the initial collision of the shock front with the deflagration front will only result in a slight deceleration of the deflagration front. It will not stop the wall, at least not at first. Once the shock has passed through the deflagration front (and heated it slightly), the hotter plasma behind the shock front will begin to influence the deflagration front. The temperature of the plasma behind the shock increases as the two neighboring bubble walls approach, and this will further slow down the deflagration front.

We can get an idea of how much a bubble wall slows down by considering the following. One generic characteristic of deflagration wall propagation is that most of the latent heat released is transported *in front* of the deflagration wall. Some of the latent heat goes toward heating the u phase, but most of the latent heat goes in front of the wall (this is borne out in numerical simulations of the previous section). Therefore, in case 3, *the released latent heat is concentrated* into a smaller volume of space, namely, the space immediately in front of the deflagration wall. This is in contrast to case 2, where the released latent heat is smoothly distributed through-

out all of space.

One major consequence of this concentration of released latent heat is that the plasma can now more easily reheat back up to T_c in these concentrated regions, and so the lower limit for L to produce significant inhomogeneities found in case 2 can now be reduced. That is to say, in case 3, a larger range of values for L will produce baryon overdensities greater than order unity.

To get an idea of which values of L will produce significant inhomogeneities, consider the following simple model. Assume that all the bubbles nucleated at the same time, with their centers (densely packed) at a distance d apart [see Eq. (53)]. The deflagration walls will travel a distance

$$r_0 = \frac{v_0 d}{v_0 + c_s} \tag{A1}$$

before encountering a shock, and the velocity of the walls will be constant (v_0) out to this distance (recall that c_s is the velocity of the shock). At the moment when the deflagration wall encounters the shock from a neighboring bubble, the volume V_u of the unit cell that is in front of the deflagration front is (therefore still in the unbroken u phase)

$$V_u = \frac{4\pi d^3}{3(c_s + v_0)^3}\left[\left(\frac{c_s + v_0}{2}\right)^3 - v_0^3\right] . \tag{A2}$$

If we assume that all of the latent heat is transported in front of the deflagration wall, then we can estimate how much latent heat is needed to reheat the plasma in front of the deflagration front back up to T_c. The total amount of energy that will go into reheating the plasma in front of the deflagration wall is $E_{\rm tot} \approx L(V_u + 4\pi r_0^3/3)$. Therefore, if

$$L\left(1 + \frac{v_0^3}{\left(\frac{c_s+v_0}{2}\right)^3 - v_0^3}\right) \gtrsim 3a(T_c^4 - T_n^4) , \tag{A3}$$

then the latent heat L is big enough to reheat the plasma such that the bubble walls will slow down considerably once they have collided with the shocks. This condition must be met in order for $\delta_B \gg 1$. The only difference between Eq. (A3) and the limit obtained in case 2 [Eq. (55)] is the factor in the parentheses on the left-hand side of (A3). This is the factor describing the concentration of the released latent heat. For low values of v_0, this factor is close to 1. As an example, for $v_0 = 0.2$, this factor $\simeq 1.16$. But for, say, $v_0 = 0.5$, this factor $\simeq 5$. For values of $v_0 > 0.5$, the factor becomes very large. This means that for large deflagration velocities the latent heat L has to be very small in order for the bubble walls to collide without slowing down first.

The scale size ℓ for the inhomogeneities in this case is

$$\ell \approx \frac{d}{2} - r_0 = \frac{d}{2}\frac{(c_s - v_0)}{(c_s + v_0)} ; \tag{A4}$$

for $v_0 \to c_s$, this can be very small (recall $d \sim 10^{-5}H^{-1}$ is already small).

Now we can put together a picture of what happens during the phase transition in case 3. At first, the nucleated bubbles travel with constant velocity v_0 until they reach a radius r_0. At this point, they collide with the shock of a neighboring bubble and begin to slow down. If the latent heat is large enough that condition (A3) is met, the bubble walls will slow down to some minimum velocity $v_{\rm min}$ (see below), and large amplitude inhomogeneities of size ℓ will form. If the latent heat is small, then inhomogeneities with an amplitude of order 1 and with size ℓ will form.

The minimum velocity of the deflagration walls can be found by using a method similar to the one used in case 2 [Eq. (56)]. First, let us assume that L is large such that condition (A3) is met. Next, let us make the assumption that the phase transition has proceeded to the point that the b phase dominates, and the remaining u phase is in the form of shrinking bubbles of radius $r_u \approx \ell$. The bubbles of the u phase have become so hot that the deflagration wall has slowed down almost to a stop. In fact, they would stop were it not for the fact that heat is being removed both by expansion of the Universe and by hydrodynamic leakage (i.e., shocks are leaking out of bubble and taking heat with them). Let us make a gross simplification and assume that the amount of heat leaking out from the shocks is equal to the amount of heat coming in from shocks of neighboring bubbles. Then the heat is only removed by the expansion of the Universe, just as in case 2. We can then estimate the minimum velocity by using the conservation of energy equation (51). In this case, we use the same assumptions that led to (56), but now $r \to r_u$ and F is the fraction of the bubble volume that remains after starting with initial radius ℓ (we set $F = 0.5$). With these assumptions, one obtains an estimate for the minimum velocity of the deflagration wall of the shrinking bubbles:

$$v_{\rm min} \approx \frac{8 r_u H}{L/aT_c^4} \approx \frac{4dH}{L/aT_c^4}\frac{c_s - v_0}{c_s + v_0} , \tag{A5}$$

where we have set $r_u \approx \ell$. This expression is similar to case 2; in fact, (A5) approaches the case 2 value as $v_0 \to 0$. The only difference between the minimum velocities for the two cases is the factor $(c_s - v_0)/(c_s + v_0)$, which accounts for the small size of the u phase bubbles. For the EW phase transition, $v_{\rm min} \sim 1\text{–}10^{-3} \times (c_s - v_0)$. If $c_s \approx v_0$, then $v_{\rm min}$ can become very small. However, as stated in Sec. X, baryon production turns off at $v \lesssim 10^{-4}$, and so $\delta_B^{\rm max}$ cannot become too large.

For the case of large L, that is, when (A3) is met, we can now estimate χ and δ_B. Estimating the baryon over density δ_B is simple. Using (52) and (A5), one obtains

$$\delta_B^{\rm max} \approx \frac{L/aT_c^4}{4dH}\frac{v_0(c_s + v_0)}{c_s - v_0} . \tag{A6}$$

The baryon enhancement factor χ can be estimated by using

$$\chi \approx \frac{(d/2)^3 - \ell^3 + \delta_B^{\rm max}\ell^3}{(d/2)^3} , \tag{A7}$$

where we have used (1) for the density of baryons. Substituting in Eqs. (A6) and (A1), one obtains

$$\chi \approx 1 + \left(\frac{c_s - v_0}{c_s + v_0}\right)^3 \left(\frac{(L/aT_c^4)}{4dH} \frac{v_0(c_s + v_0)}{c_s - v_0} - 1\right) . \quad \text{(A8)}$$

As a reminder, Eq. (A8) is an estimate of the baryon enhancement for case 3 assuming that condition (A3) is met, so that the deflagration walls slow down to a minimum determined by the expansion rate of the Universe. There is one subtle difficulty in calculating Eq. (A8), and that is in finding the average bubble spacing d. In Sec. VI we discuss the behavior of d in the case of homogeneous heating (case 2), and we will find that although d is a function of time, is has an asymptotic value. For the same reasons as in case 2 (namely, reheating), case 3 will also have an asymptotic value of d. In order to simplify matters, we will then use this asymptotic value for d obtained using case 2 in Eq. (A8). The numerical results of our case 3 estimate of χ are included in Sec. VI.

[1] A. Cohen, D. Kaplan, and A. Nelson, Annu. Rev. Nucl. Part. Sci. **43**, 27 (1994).
[2] K. Kajantie and H. Kurki-Suonio, Phys. Rev. D **34**, 1719 (1986).
[3] J. Ignatius, K. Kajantie, H. Kurki-Suonio, and M. Laine, Phys. Rev. D **49**, 3854 (1994).
[4] V. Kuzmin, V. Rubakov, and M. Shaposhnikov, Phys. Lett. **155B**, 36 (1985).
[5] A. Nelson, D. Kaplan, and A. Cohen, Nucl. Phys. **B373**, 453 (1992).
[6] M. Joyce, T. Prokopec, and N. Turok, Phys. Lett. **B 338**, 269 (1994).
[7] A. Cohen, D. Kaplan, and A. Nelson, Phys. Lett. B **263**, 86 (1991).
[8] M. Dine and S. Thomas, Phys. Lett. B **328**, 73 (1994).
[9] S. Coleman and E. Weinberg, Phys. Rev. D **7**, 1888 (1973).
[10] A. Linde, Nucl. Phys. **B216**, 421 (1983).
[11] M. Dine *et al.*, Phys. Rev. D **46**, 550 (1992).
[12] G. Anderson and L. Hall, Phys. Rev. D **45**, 2685 (1992).
[13] M. Shaposnikov, Phys. Lett. B **277**, 324 (1992); **282**, 483(E) (1992).
[14] M. Carrington, Phys. Rev. D **45**, 2933 (1992).
[15] P. Arnold and O. Espinosa, Phys. Rev. D **47**, 3546 (1993).
[16] M. Carrington and J. Kapusta, Phys. Rev. D **47**, 5304 (1993).
[17] J. Langer, Ann. Phys. (N.Y.) **54**, 258 (1969).
[18] S. Coleman, Phys. Rev. D **15**, 2929 (1977).
[19] A. Guth and E. Weinberg, Phys. Rev. D **23**, 876 (1981).
[20] J. Ignatius, Ph.D. thesis, University of Helsinki, 1993.
[21] L. Landau and E. Lifshitz, *Fluid Mechanics* (Pergamon, Oxford, 1982).
[22] R. Courant and K. Friedrichs, *Supersonic Flow and Shock Waves* (Springer-Verlag, Berlin, 1985).
[23] H. Kurki-Suonio, Nucl. Phys. **B255**, 231 (1985).
[24] M. Laine, Phys. Rev. D **49**, 3847 (1994).
[25] B. H. Liu, L. McLerran, and N. Turok, Phys. Rev. D **46**, 2668 (1992).
[26] P. Arnold, Phys. Rev. D **48**, 1539 (1993).
[27] N. Turok, Phys. Rev. Lett. **68**, 1803 (1992).
[28] H. Goldstein, *Classical Mechanics*, 2nd ed. (Addison-Wesley, Reading, MA, 1980).
[29] M. Gyulassy, K. Kajantie, H. Kurki-Suonio, and L. McLerran, Nucl. Phys. **B237**, 477 (1984).
[30] K. Enqvist, J. Ignatius, K. Kajantie, and K. Rummakainen, Phys. Rev. D **45**, 3415 (1991).
[31] H. Kurki-Suonio, Phys. Rev. D **37**, 2104 (1988).
[32] T. Walker, D. Schramm, K. Olive, and H. Kang, Astrophys. J. **376**, 51 (1991).
[33] G. Fuller, G. Mathews, and C. Alcock, Phy. Rev. D **37**, 1380 (1988).
[34] K. Jedamzik, G. Fuller, and G. Mathews, Astrophys. J. **423**, 50 (1994).
[35] A. Heckler and C. Hogan, Phys. Rev. D **47**, 4256 (1993).
[36] K. Jedamzik and G. Fuller, Astrophys. J. **423**, 33 (1994).
[37] G. Fuller, K. Jedamzik, G. Mathews, and A. Olinto, Phys. Lett. B **333**, 135 (1994).
[38] Ideas for this section came from discussions with Craig Hogan.
[39] U. Yajnik, Phys. Rev. D **34**, 1237 (1986).